Size-Dependent Electronic Structure of Titanium-Oxo-Alkoxides: Quantum Confinement at the Smallest Sizes.

Thomas J. Barnes,[a] Bin Wang,[b] Eniola Sokalu,[a] Frank De Proft,[b]* Sebastian D. Pike [a]*

a) Department of Chemistry, University of Warwick, Coventry, UK

b) Research Group of General Chemistry (ALGC), Vrije Universiteit Brussel (VUB), Pleinlaan 2, B-1050 Brussels, Belgium

Supporting Information

Contents

Experimental methods

'Anhydrous' toluene and THF was purchased from Sigma Aldrich, 'extra-dry' dichloromethane was purchased from Fisher Scientific. All air-free solvents were prepared by degassing by three freeze-pump-thaw cycles or by bubbling with N_2 for 30 minutes and stored over 4 Å molecular sieves. d_8-toluene was dried by stirring over CaH_2 and vacuum distilled using grease-free trap-to-trap apparatus, before storing over 4 Å molecular sieves under nitrogen. Molecular sieves were activated before use by heating under vacuum (>150°C) until the head space partial pressure was less than 10^{-1} mbar. Moisture analysis of prepared solvents was conducted by Karl Fischer spectrometric analysis: pentane, 3.0 ppm; toluene, 5.6 ppm; THF, 10.7 ppm; MeCN, 8.4 ppm; dichloromethane 4-6 ppm.

$[Ti(OMe)_4]_4$ was stored in a N_2 filled glovebox and used directly as supplied by Sigma Aldrich. Liquid titanium alkoxides $[\{Ti(OEt)_4\}_n]$ ('purum' or 'for synthesis', Sigma Aldrich), $[Ti(O^iPr)_4]$ (≥97%, Sigma Aldrich) and $[Ti(O^tBu)_4]$ (98%, Thermo Scientific) respectively. Commercial samples of $[\{Ti(OEt)_4\}_n]$ contained between 2-17% of alkoxides as O^iPr by ^1H NMR spectroscopy (Fig S3) depending on grade of purity ('purum' 2%, 'for synthesis' 17%), however, the UV/vis spectra and DOSY NMR spectra of different batches were very similar and this was not deemed an important factor. Liquid titanium tetra-alkoxides ($[\{Ti(OEt)_4\}_n]$, $[Ti(O^iPr)_4]$, $[Ti(O^tBu)_4]$) were distilled using a grease free trap-to-trap apparatus and stored in the glovebox prior to collecting UV/vis spectra (Fig. S1).

Note that commercially supplied $[Ti(O^iPr)_4]$, often with a pale-yellow colour, likely contains some larger nuclearity Ti-oxo-alkoxide clusters from trace hydrolysis (even if stored under air-free conditions) or other impurities such as halides. We have previously reported the energy gap of commercial grade $[Ti(O^iPr)_4]$ (without a distillation purification) as 3.74 ± 0.2 eV, however, this is likely to be an under-estimate due to the presence of these impurities.[1]

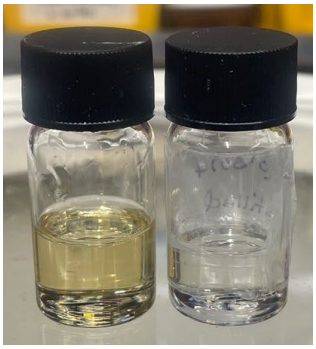

Figure S1. Photograph of $[Ti(O^iPr)_4]$ before and after vacuum distillation

$[Ti(OAd)_4]$ was prepared following an amended procedure.[2] $Ti(O^iPr)_4$ (1.04 mL, 3.52 mmol) and 1-adamantanol (2.14 g, 14.1 mmol) were dissolved in 20 mL of dry toluene under a nitrogen atmosphere. The reaction was heated to reflux for 2 hours and left to stand for 2 days. Large, colourless blocks of $[Ti(OAd)_4]$ were isolated from the side of the flask (470 mg, 21%). The structure was confirmed by X-ray crystallography – consistent with a previously reported structure.

Ti_3,[3] **Ti_7**,[4] **Ti_{11}**,[5] **Ti_{12}**,[5] **Ti_{16}**,[6] **Ti_{17}**[7] and **Ti_{18}**[8] were prepared as crystalline solids using literature procedures and the expected structures confirmed by X-ray crystallography. Solution NMR spectroscopy was used to determine bulk purity for all except **Ti_3**, which is known to form an equilibrium with larger clusters in solution.

Summary of previously reported Ti-oxo-alkoxide synthesis: Adding a small quantity of water (<0.05 equivalents) to a solution of $[Ti(OR)_4]$ promotes formation of $[Ti_3O(OR)_{10}]$ clusters via hydrolysis and condensation reactions (in equilibrium with $[Ti(OR)_4]$).[3] By adding MeOH, the compound $[Ti_3O(O^iPr)_9(OMe)]$ (**Ti_3**) can be isolated as a crystalline product, however, forms an equilibrium with higher nuclearity clusters and $[Ti(O^iPr)_4]$ when in solution. Addition of further equivalents of water generates larger clusters (e.g. $[Ti_7O_4(OEt)_{20}]$ (**Ti_7**, Fig. 1),[9] forming a maximum metastable size under room-temperature hydrolysis conditions in alcohol solvent (e.g. $[Ti_{11}O_{13}(O^iPr)_{18}]$) (**$Ti_{11}$**, Fig. 1).[10] Introducing heating, can increase cluster size (e.g. $[Ti_{12}O_{16}(O^iPr)_{16}]$),[5] whilst employing solvothermal conditions, allows growth of even larger clusters (e.g. $[Ti_{16}O_{16}(OEt)_{32}]$ (**Ti_{16}**), $[Ti_{17}O_{24}(O^iPr)_{20}]$ (**Ti_{17}**) and $[Ti_{18}O_{28}H(O^tBu)_{17}]$) (**$Ti_{18}$**) (Fig. 1).[6-8]

UV-visible spectroscopy

Solution UV-visible spectroscopy was recorded using a Implen NanoPhotometer C40 or a Shimadzu 2600i, using a bespoke Young's tap cuvette for air free analysis.

Diffuse reflectance (solid-state) UV-visible-NIR spectroscopy (DRS) was carried out on a Shimadzu 2600i fitted with an integrating sphere attachment. Samples were prepared in a quartz window cell with the sample placed inside a 1 mm deep PTFE washer and the cell sealed with PTFE tape on the threads. Alternatively, samples were loaded into a 0.5 mm deep quartz cell sealed inside a glovebox with a quartz plate by vacuum grease to ensure air-tight conditions. Comparison of the two methods of preparing cells gave similar results, noting that the most air-sensitive compounds such as $[Ti(OAd)_4]$ show a notable change in spectra over the course of hours once removed from the glovebox but retained within the cell. The Kubelka-Munk function was used to derive absorption over scattering and subtracted from a background of $BaSO_4$ (collected in the same cell as the

experiment). The sample of $BaSO_4$ is shared between measurements to minimise variations in the measurement of the background.

The absorption onset is described by: $A = B(hv - Eg)^n / hv$ Where A is absorption, B is the absorption constant for the transition, Eg is the energy gap in eV and hv is the photon energy. The exponent n is given a value of 3 for solution data (for a forbidden indirect transition, following literature precedent[11]), 2 for solid-state data (for an indirect transition) and 0.5 for a direct transition in solution or solid state. A plot of $(Ahv)^{1/n}$ vs hv gives a straight line, and the intercept of this line with the baseline of the data is attributed to the absorption onset.

Solution concentrations are defined as concentration of Ti atoms, [Ti], to normalise the varying Ti nuclearities in different species. Solution spectra (in pentane) were analysed at [Ti] = 35 mM and 1.75 mM using an exponent of n = 3, a linear section ($R^2 \geq 0.97$) beginning from absorption = 2 (named *straight line* in plots) was extrapolated to the fitted baseline (named *flat line* in plots).[1, 11-13] Low concentration data at [Ti] = 0.11 mM were analysed using an exponent of n = 0.5, a linear section ($R^2 \geq 0.97$) that includes the inflection point of the curve was extrapolated to the fitted baseline.[11]

Solid-state (DRS) UV/visible data was analysed using n = 2 and 0.5 exponents, to be consistent with studies of bulk TiO_2, a linear section ($R^2 \geq 0.97$) that includes the inflection point of the curve was extrapolated to the fitted baseline. The point of absorption onset (in eV) was derived at the x-value of the intercept of the straight line with a straight line describing the baseline (to avoid any error from extrapolating through an imperfect baseline).[14]

Electrochemistry

The electrochemical measurements were conducted using a Metrohm Autolab PGSTAT204 potentiostat using the supplied NOVA software.

Cyclic voltammetry measurements were conducted using extra-dry dichloromethane (DCM), which was further dried over 4 Å molecular sieves. Tetrabutylammonium hexafluorophosphate ($[NBu_4][PF_6]$) was used as the supporting electrolyte, at a 0.1 M concentration. The supporting electrolyte solution was further dried over 4 Å molecular sieves and tested by Karl Fisher titration to verify a low water content of 4-6 ppm.

Electrochemistry was carried out in three-electrode potentiostatic arrangement where boron-doped diamond (BDD) was the working electrode, Pt wire was used as the counter electrode and polished Ag wire served as a pseudo-reference electrode. BDD was selected as the working electrode due to its low background and capacitive currents in addition to its large solvent window allowing for scanning in >3.5 V potential range.[15] All measurements were carried out in air-free conditions inside a N_2 filled glovebox. High quality electro-analytical grade BDD (MR14, 3 mm, Element Six Ltd., Oxford, UK) was used as the working electrode across all measurements. The negligible sp^2 diamond was doped with boron (>10^{20} B atoms cm^{-3}) to allow for conductive metallic-like behaviour. The 3 mm BDD disks were contacted with a brass rod and finally encapsulated using Rigid10k epoxy resin (PMMA/Glass, FormLabs). An extended electrical connection was made to the made to the BDD macro electrode by soldering copper wire to the brass rod (the copper wire and soldered connection were both insulated). This was done to maintain a constant connection between the WE and the potentiostat.

The BDD electrodes were cleaned electrochemically by both applying a large oxidative potential (3 V *vs.* Ag/AgCl 3 M NaCl) in pulsed chronoamperometric measurements (5 s) in a 1 M

$HClO_4$ electrolyte solution. This was done to remove adsorbed species from the electrode surface. The electrode was pulsed 10 times, removed from the electrochemical setup. Following electrochemical cleaning the solvent window of the electrode was explored in degassed 0.1 M KNO_3 between -2 and +2 V at a scan rate of at 100 $mV \cdot s^{-1}$ for three consecutive cycles. Following this the electrode was rinsed with ultrapure water, dried on a lint-free cloth and was stored in an 80 °C oven until use.

The BDD working electrode surface was prepared by cleaning the electrode on a microfibre polishing pad in an alumina (Al_2O_3)/MilliQ water slurry, and cleaned once again on a polishing pad with only water, after which the BDD surface was thoroughly rinsed with water. The BDD electrodes were cleaned in this manner before and after every measurement.

Electrochemical measurements in organic media were carried out in a three-electrode potentiostatic arrangement in a three-necked borosilicate glass cell. A supporting electrolyte of 0.1 M $[NBu_4][PF_6]$/DCM was made up in air-sensitive conditions using a Schlenk line and the resultant electrolyte was analysed by Karl Fischer titration to determine the water content in the solution prior to use (4-6 ppm water). The supporting electrolyte (20 mL) was injected into the electrochemical cell, and the solvent window of the electrode was explored by CV to ensure that there were no contaminants on the electrode surface and to check the working electrode capacitance and resistance.

Compounds were dissolved in dry DCM at a 1 mM concentration (treating the formula for all Ti-alkoxides as $[Ti(OR)_4]$). This solution (5 mL) was injected into the cell containing the supporting electrolyte. CV measurements were carried out on this solution (0.08 M $[NBu_4][PF_6]$, 0.2 mM [compound]), and following investigation, 1 mL of 1 mM ferrocene in DCM was added to the cell to be able to reference the peaks seen in the electrochemical measurements to the ferrocene/ferrocenium (Fc/Fc^+) redox couple.

Single Crystal X-ray Diffraction

Single crystal X-ray diffraction was carried out on a Rigaku Oxford Diffraction Synergy S diffractometer equipped with a HyPix-6000HE Hybrid Photon Counting Detector. An Oxford Cryosystems Cobra Plus system was used to cool the crystals to 100 K under a stream of N2. Single crystal X-ray diffraction structures were solved using Superflip and refined using Crystals.

Powder X-ray diffraction

PXRD patterns were collected on a Panalytical Empyrean with a Cu anode source in reflection geometry.

Nuclear Magnetic Resonance Spectroscopy

NMR spectroscopy was carried out on either a Bruker Avance III 400 MHz spectrometer or a Bruker Avance NEO 400 MHz spectrometer. All data is reported in ppm and referenced to the position of a known solvent peak. All DOSY NMR spectra were acquired on a Magritek Spinsolve 80 Carbon Benchtop NMR spectrometer equipped with a z-axis gradient coil capable of generating a maximum field gradient of 500 mT/m. DOSY spectra were interpreted using the GNAT, version 1.3.2, developed by the Manchester NMR Methodology Group.

Elemental analysis

CHN analysis was carried out by Orla McCullough at London Metropolitan University.

Characterisation of compounds

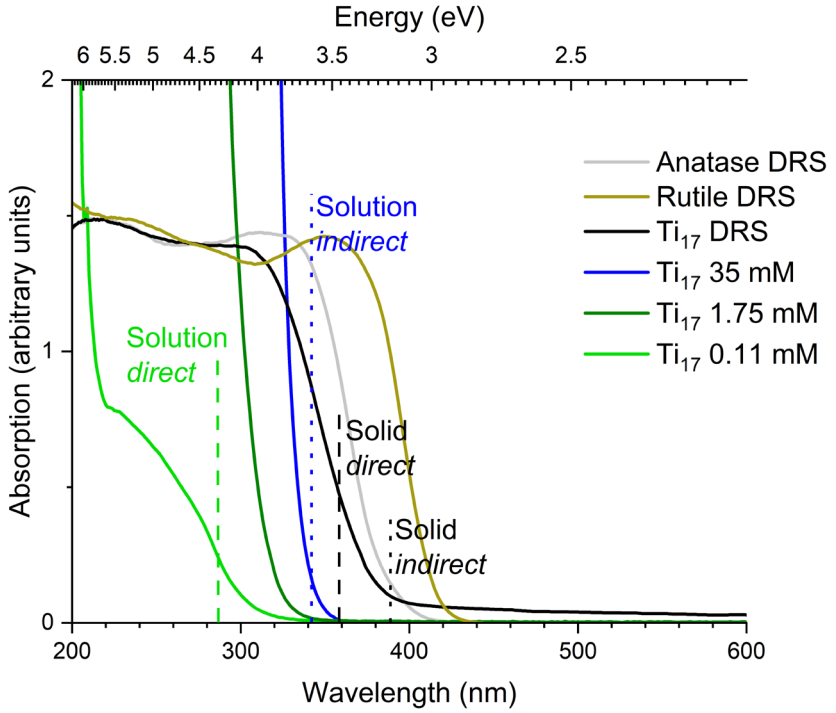

Figure S2. Absorption spectra of **Ti_{17}** in solution at three concentrations and in the solid-state, with anatase and rutile also shown. The dashed and dotted lines indicate the determined absorption onset for direct and indirect transitions respectively from Tauc's analysis of the DRS spectrum or high concentration (indirect) *and low concentration (direct)* solution data.

Table S1. Summary of the speciation of titanium tetra-alkoxides.

Titanium alkoxide	Solid-state structure	Liquid-phase structure	Solution-phase structure
$Ti(OMe)_4$	Tetramer	n/a	Monomer/Dimer/Trimer
$Ti(OEt)_4$	Tetramer	n/a	Monomer/Dimer/Trimer
$Ti(O^iPr)_4$	n/a	Monomer/Dimer	Monomer/Dimer
$Ti(O^nBu)_4$	n/a	Trimer	Monomer/Dimer/Trimer
$Ti(O^tBu)_4$	n/a	Monomer	Monomer
$Ti(ONp)_4$	Dimer	n/a	Monomer
$Ti(OAd)_4$	Monomer	n/a	n/a

The solution speciation of the tetra-alkoxides has been explored in the literature using cryoscopy, NMR spectroscopy and XANES/EXAFS.[16-18] $Ti(OEt)_4$, $Ti(OMe)_4$ and $Ti(O^nBu)_4$ were shown to have an equilibrium between monomeric, dimeric and trimeric oligomers in a benzene solution, with the trimeric form being dominant at room temperature at Ti concentrations of 3-66 mM.[16, 17] The bulkier alkoxides, $Ti(O^iPr)_4$ and $Ti(O^tBu)_4$ are mostly monomeric in solution (in range 3-16 mM) but $Ti(O^iPr)_4$ has a degree of dimerisation.[17, 18]

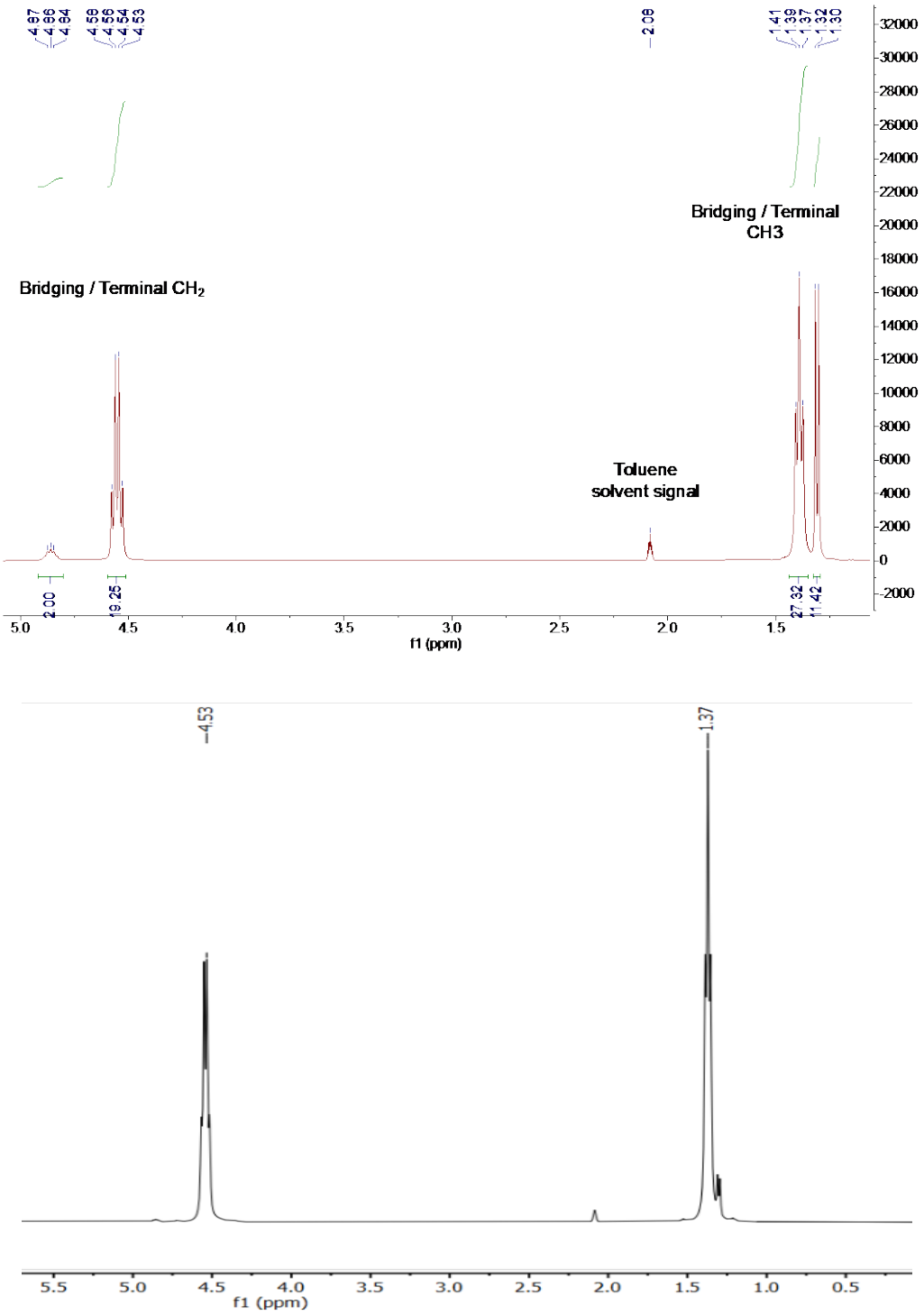

Figure S3. ^{1}H NMR of two batches of [{Ti(OEt)$_4$}$_n$] in d_8-toluene, displaying ~17 and 2% O^{i}Pr impurity respectively.

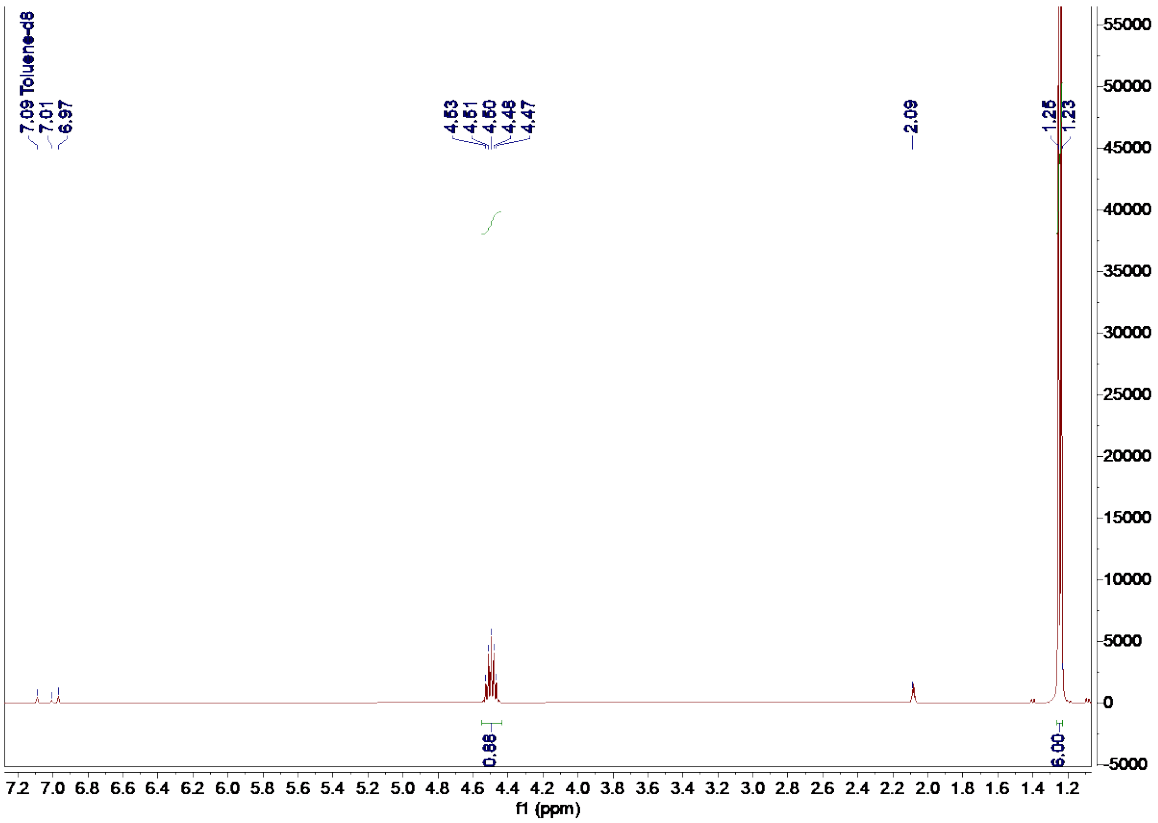

Figure S4. ^{1}H NMR spectrum of [Ti(O^{i}Pr)$_4$] in d$_8$-toluene.

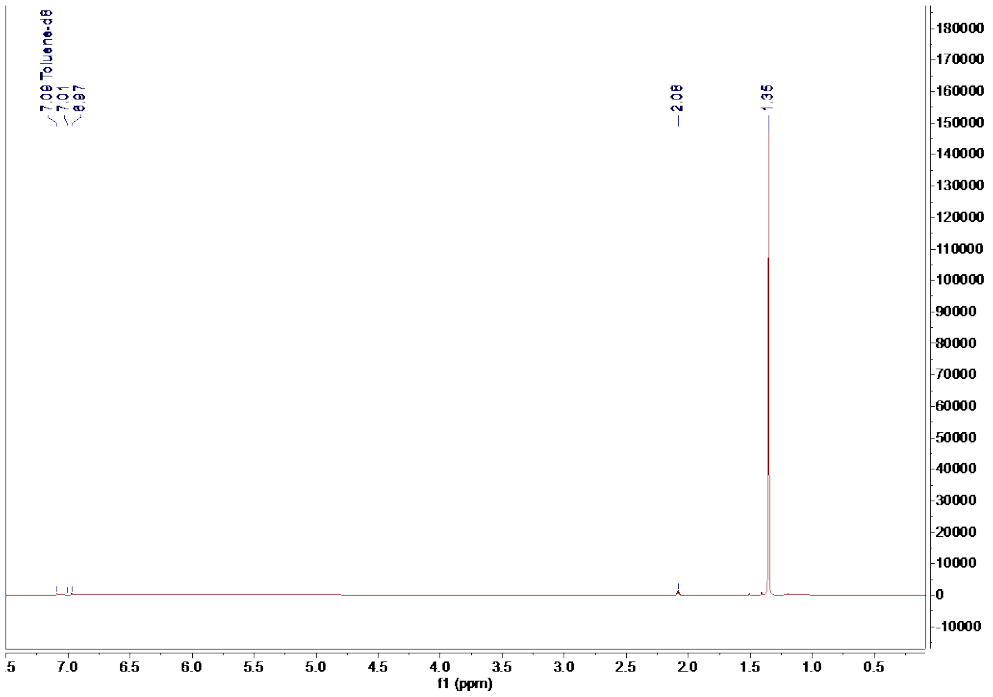

Figure S5. ^{1}H NMR spectrum of [Ti(O^{t}Bu)$_4$] in d$_8$-toluene.

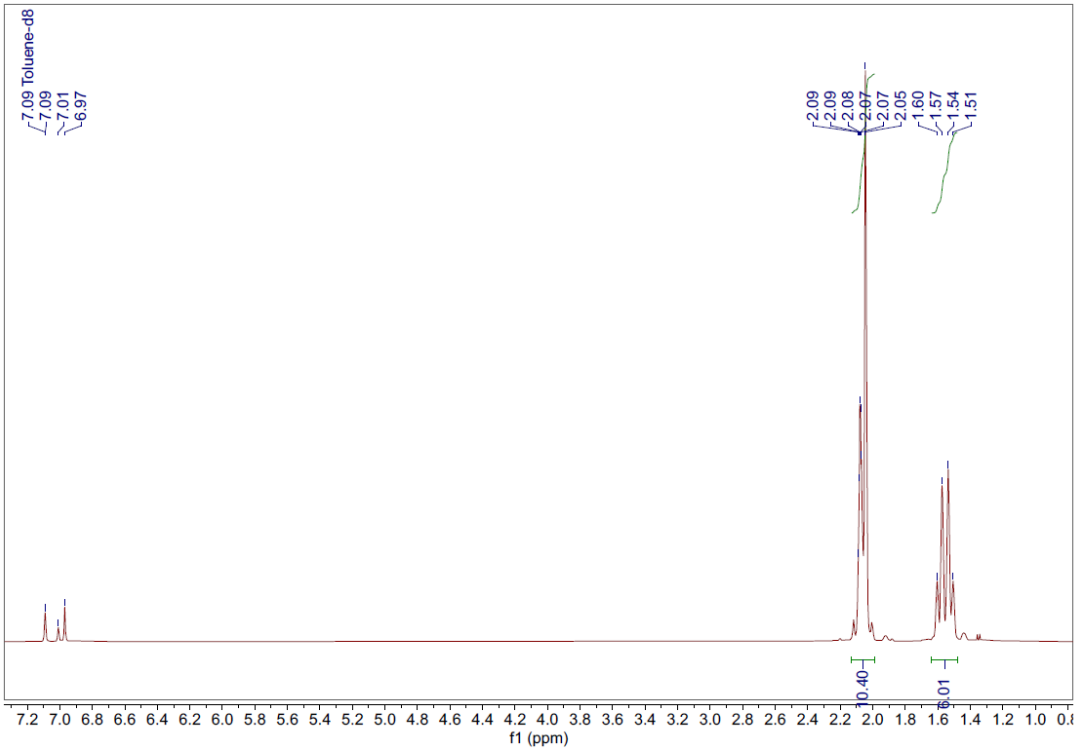

Figure S6. ^{1}H NMR spectrum of [Ti(OAd)$_4$] in d_8-toluene. N.B. residual toluene signals overlap with signal at 2.07 ppm.

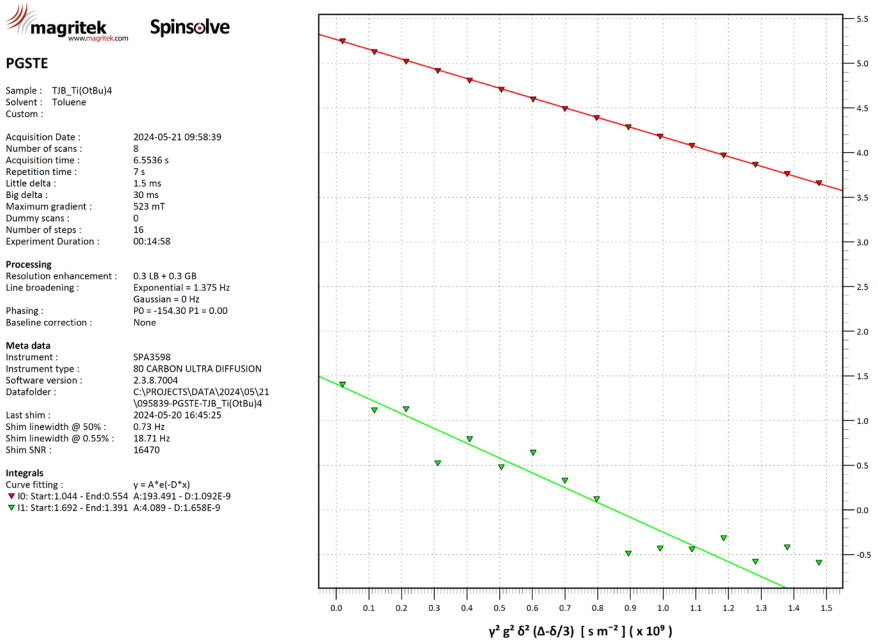

Figure S7. ^{1}H DOSY NMR fittings (80 MHz) for [Ti(O^{t}Bu)$_4$] ([Ti] = 29 mM) in d$_8$-toluene: red, compound; green, solvent.

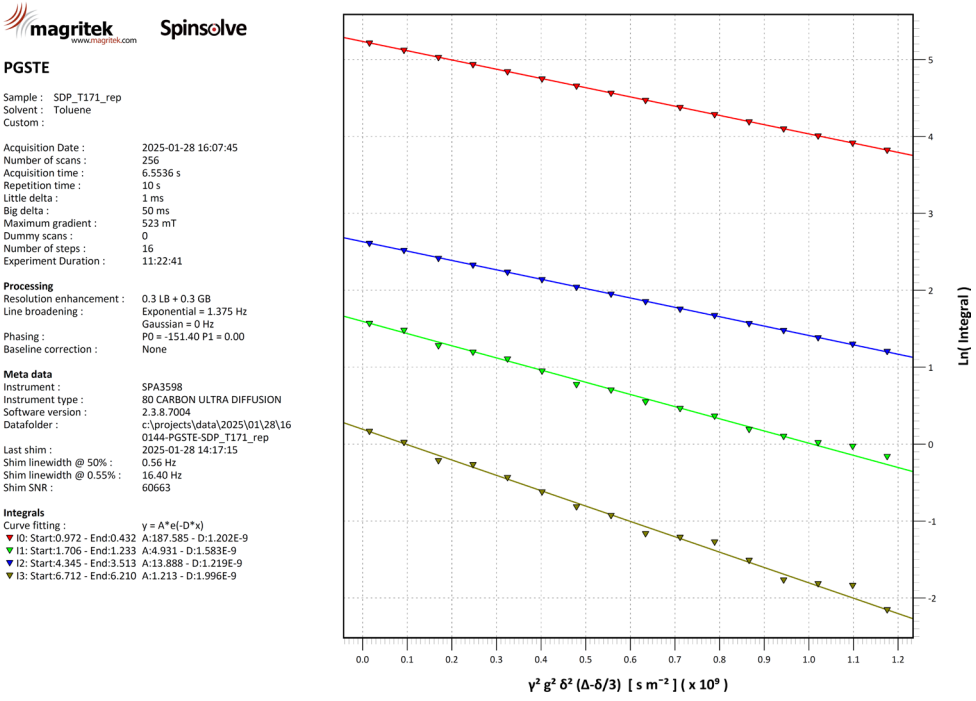

Figure S8. ^{1}H DOSY NMR fittings (80 MHz) for [Ti(O^{i}Pr)$_4$] ([Ti] = 1.8 mM) in d$_8$-toluene: red & blue, compound; green and brown, solvent.

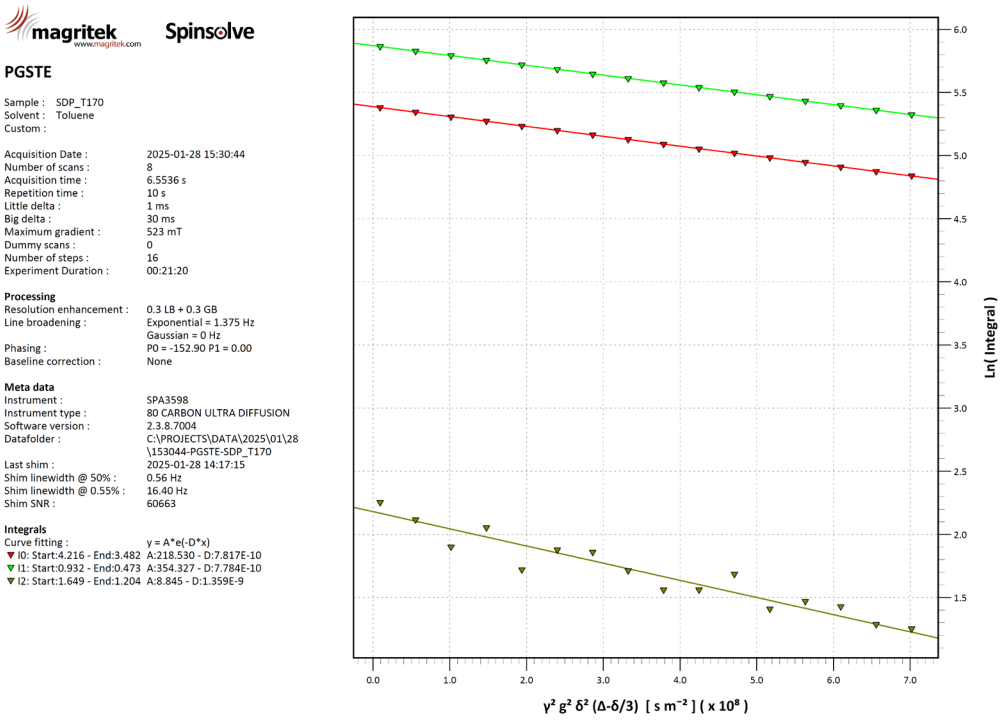

Figure S9. ^{1}H DOSY NMR fittings (80 MHz) for $[Ti(OEt)_4]_n$ ([Ti] = 35 mM) in d_8-toluene: red & green, compound; brown, solvent.

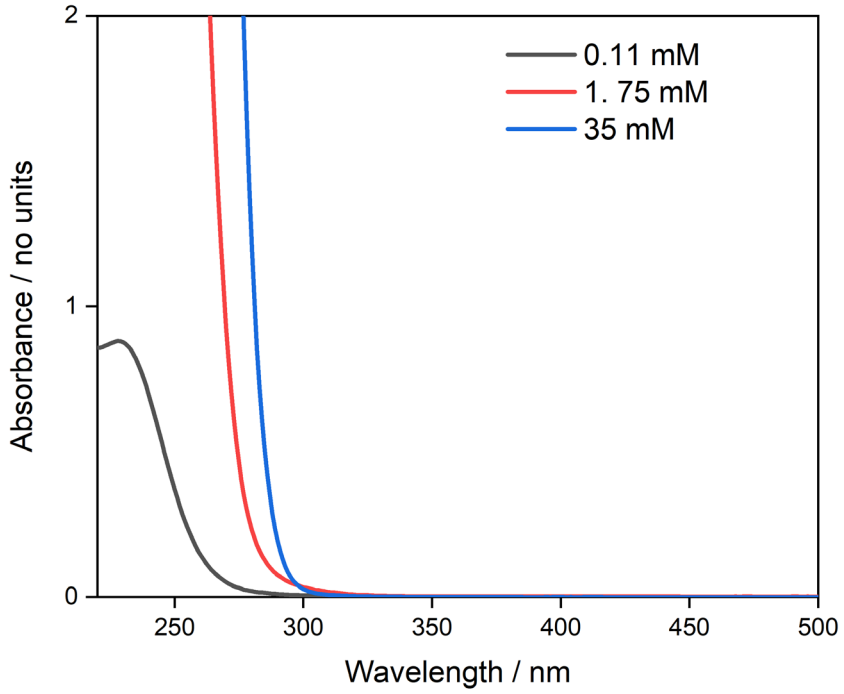

Figure S10. Absorption spectra of $[Ti(O^tBu)_4]$ in pentane solution over a range of concentrations.

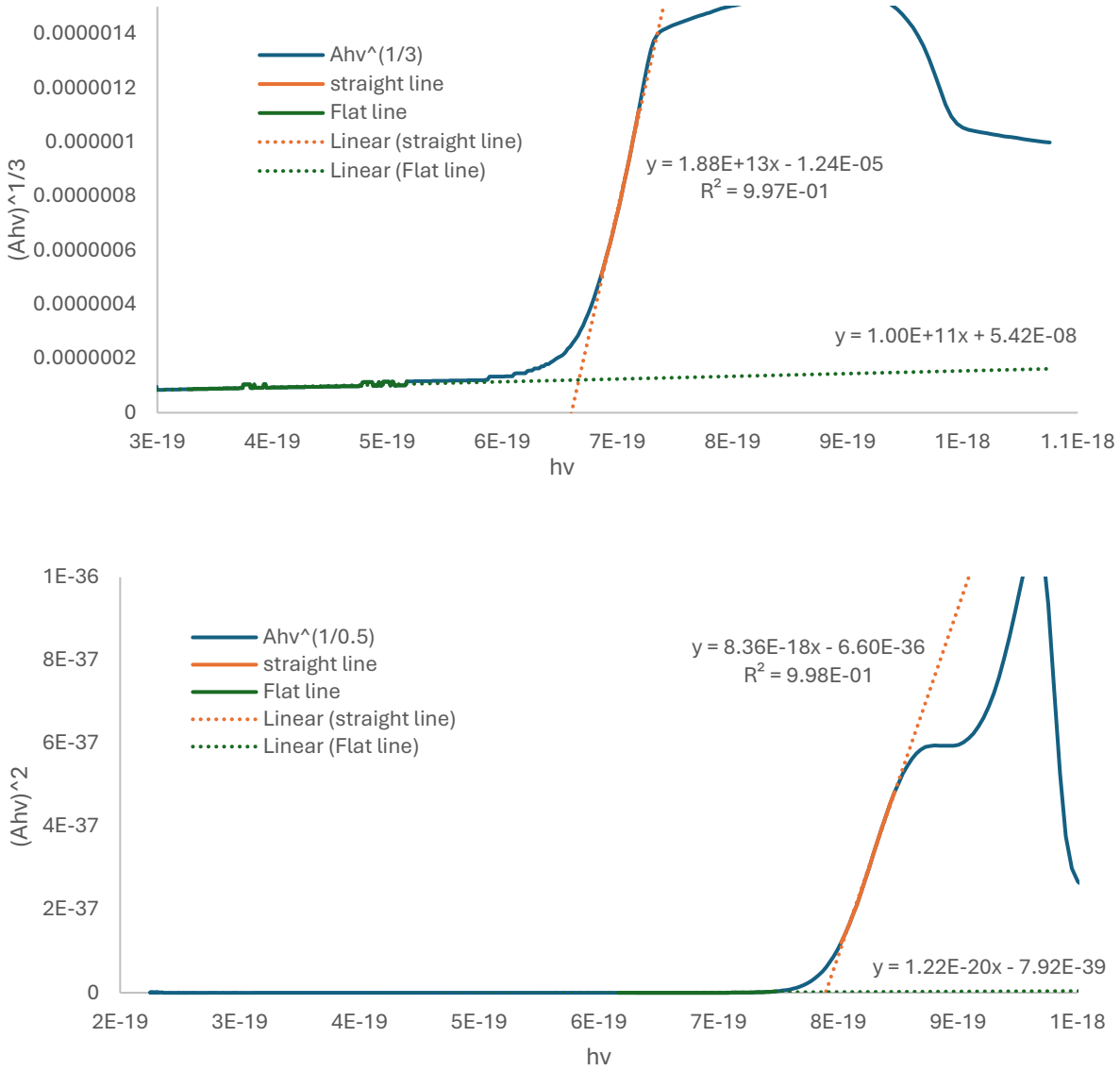

Figure S11. Tauc plots [Ti(O^tBu)$_4$] in solution, top [Ti] = 35 mM n = 3, bottom [Ti] = 0.11 mM n = 0.5. Flat line is extrapolation of baseline.

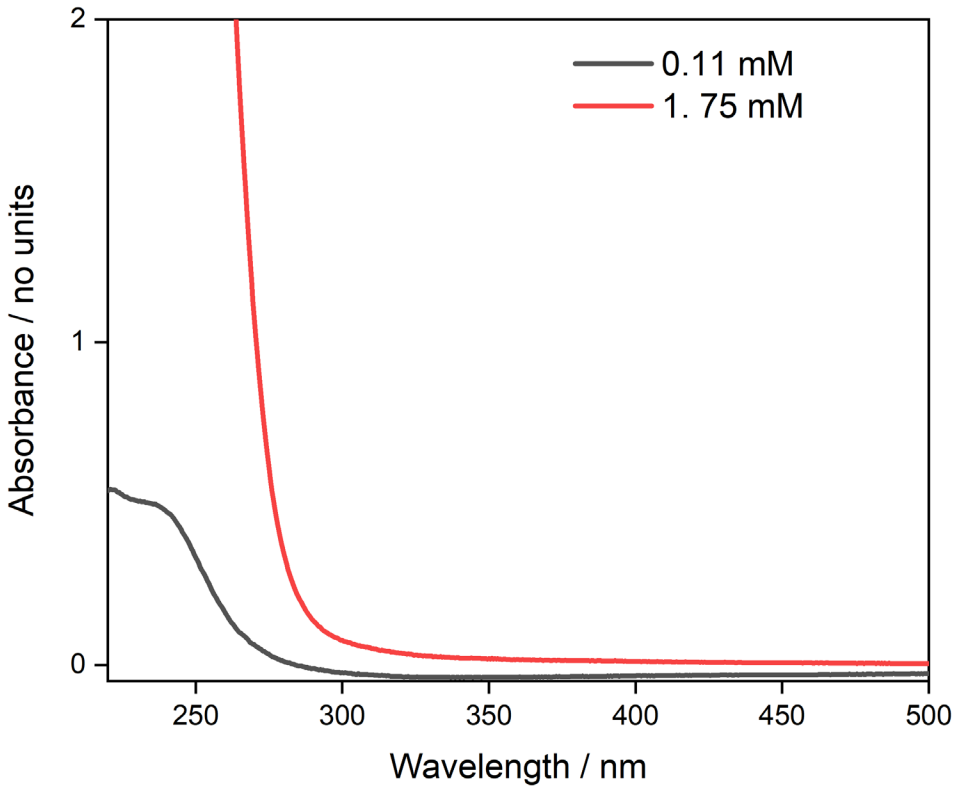

Figure S12. Absorption spectra of [Ti(OAd)$_4$] in pentane solution over two concentrations.

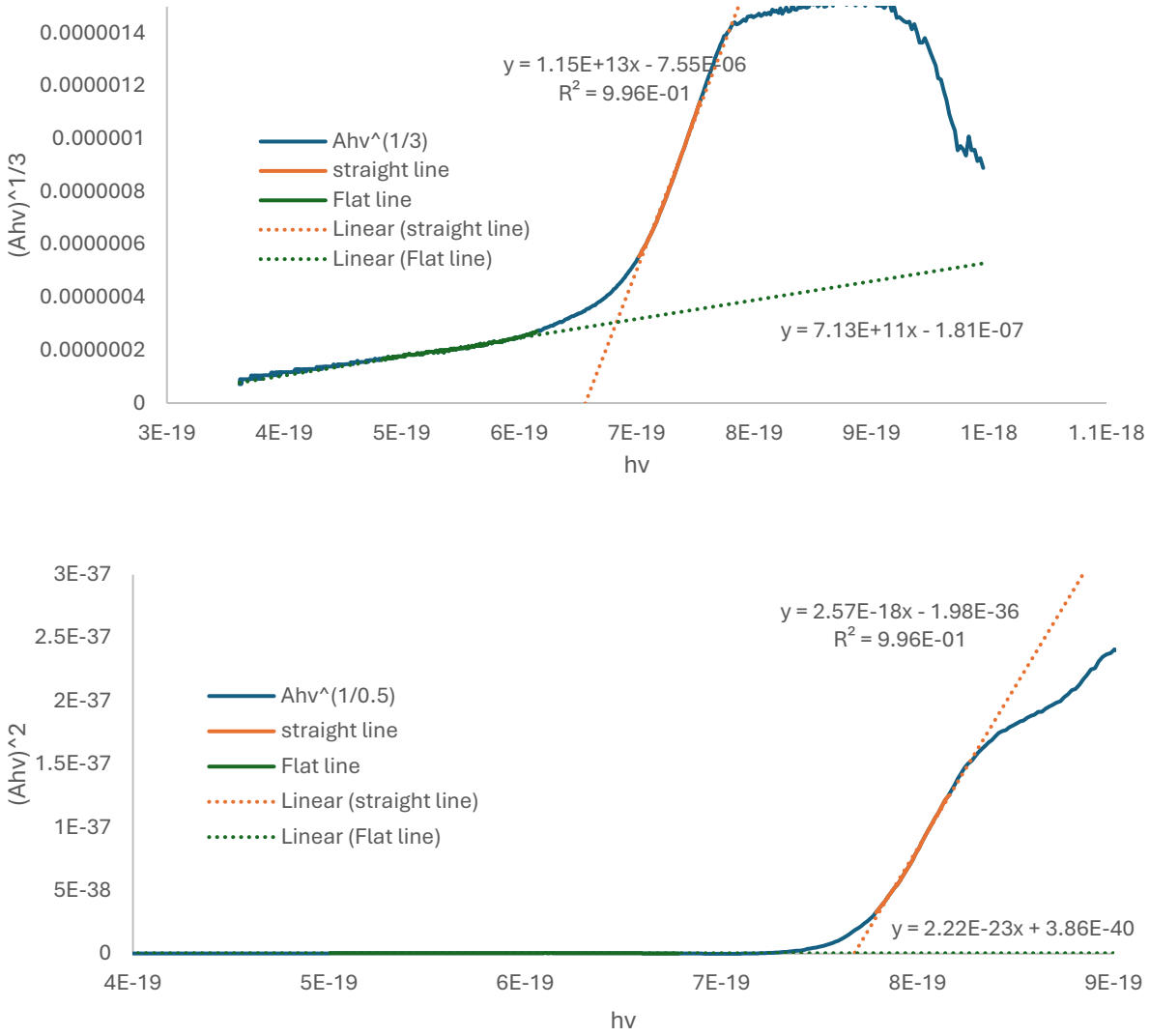

Figure S13. Tauc plots $[Ti(OAd)_4]$ in solution, top [Ti] = 1.75 mM n = 3, bottom [Ti] = 0.11 mM n = 0.5. Flat line is extrapolation of baseline.

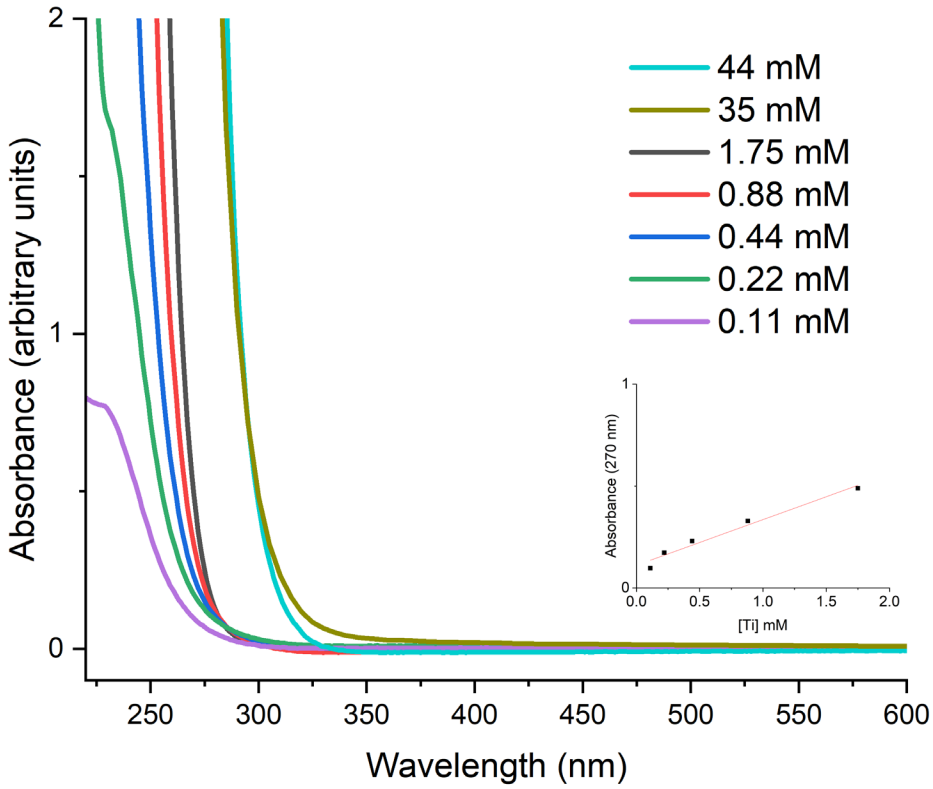

Figure S14. Absorption spectra of $[Ti(O^iPr)_4]_n$ in solution over a range of concentrations. Inset shows absorbance at 270 nm vs concentration plot.

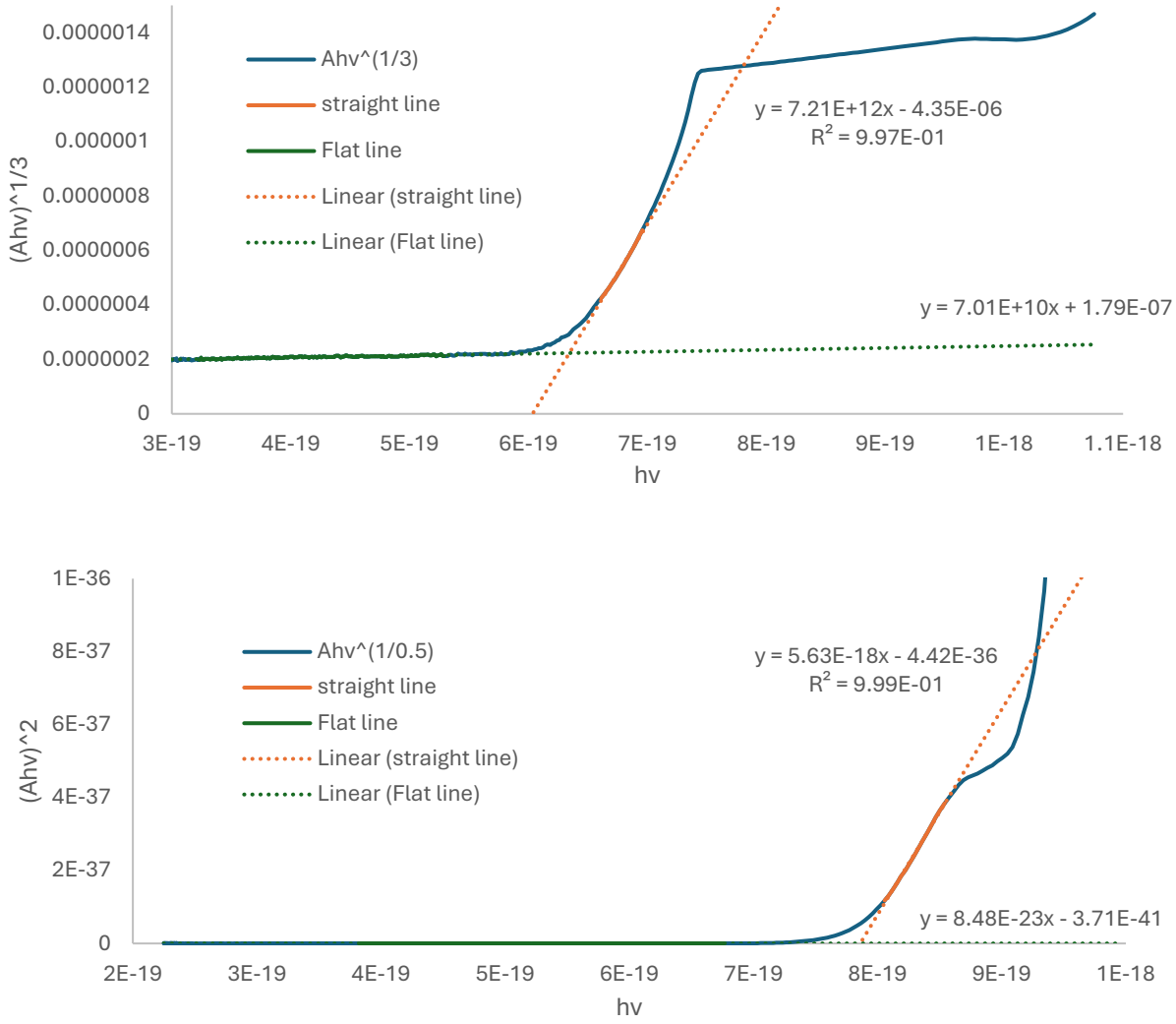

Figure S15. Tauc plots [Ti(O^iPr)$_4$] in solution, top [Ti] = 35 mM n = 3, bottom [Ti] = 0.11 mM n = 0.5. Flat line is extrapolation of baseline.

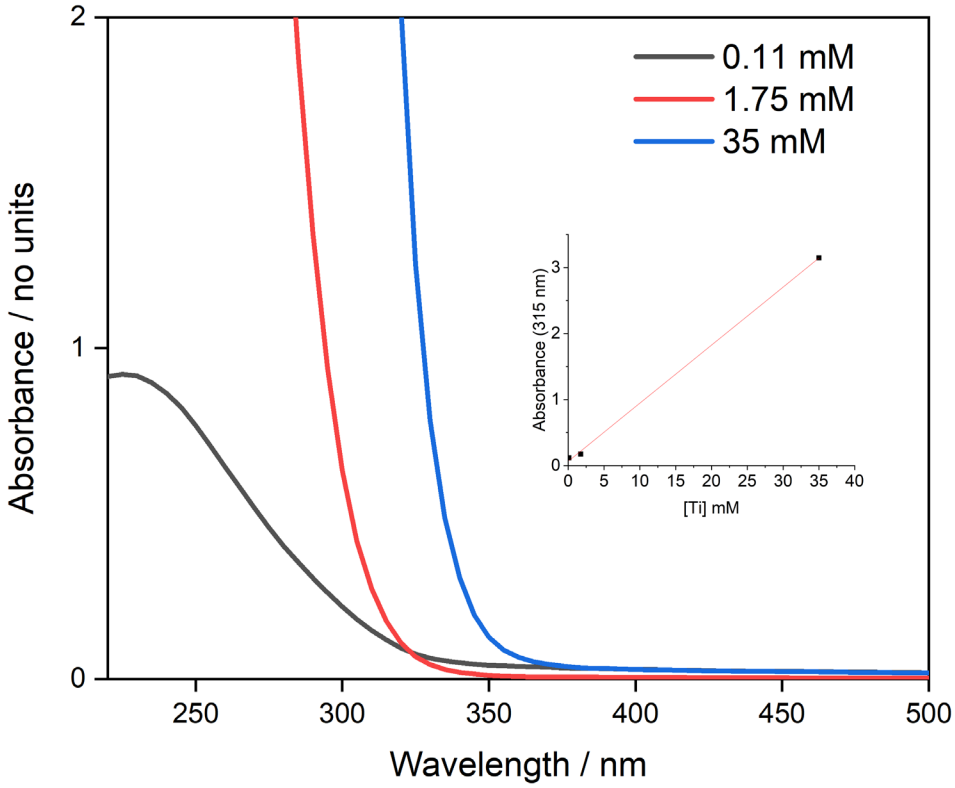

Figure S16. Absorption spectra of $[Ti(OEt)_4]_n$ in solution over a range of concentrations.

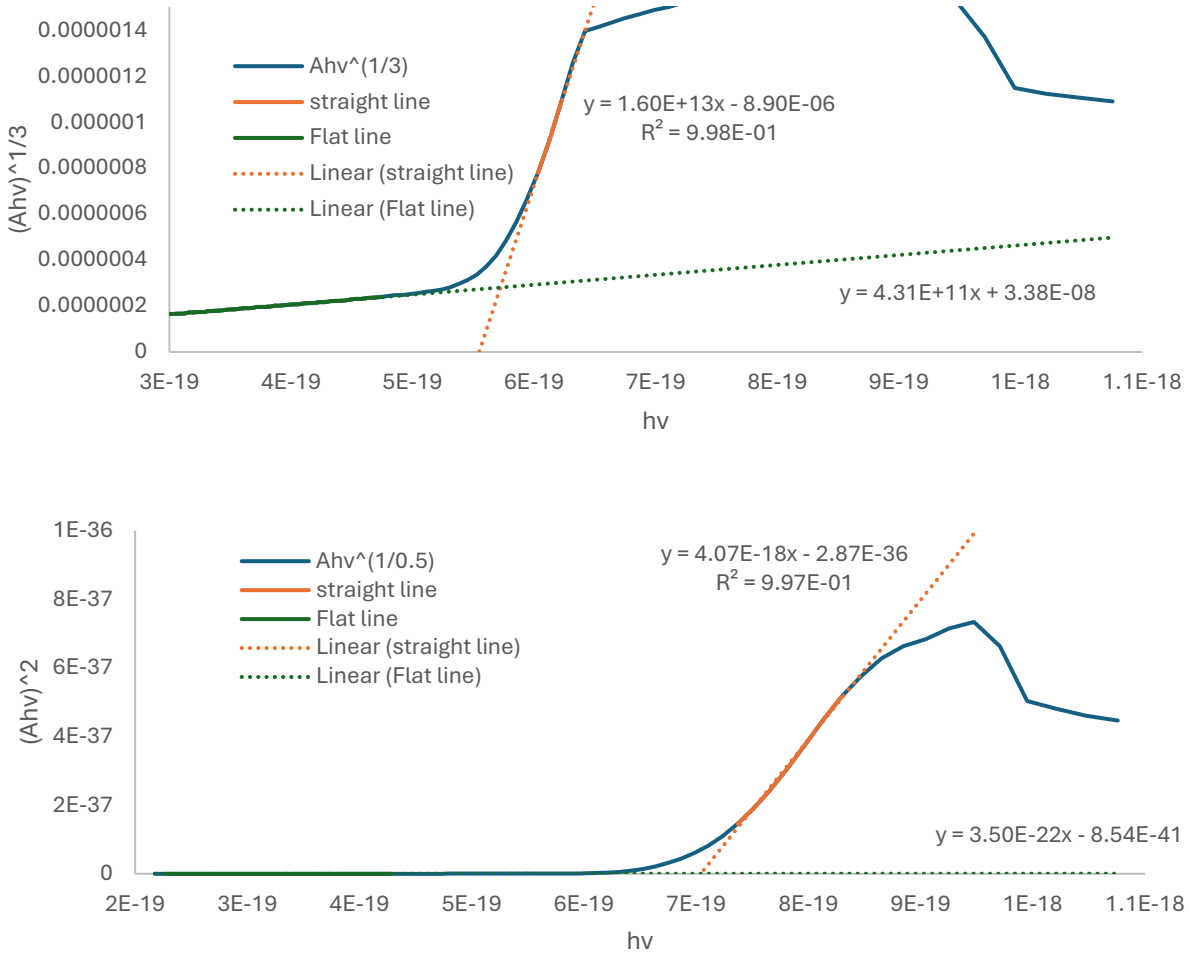

Figure S17. Tauc plots [{Ti(OEt)$_4$}$_n$] in solution, top [Ti] = 35 mM n = 3, bottom [Ti] = 0.11 mM n = 0.5. Flat line is extrapolation of baseline.

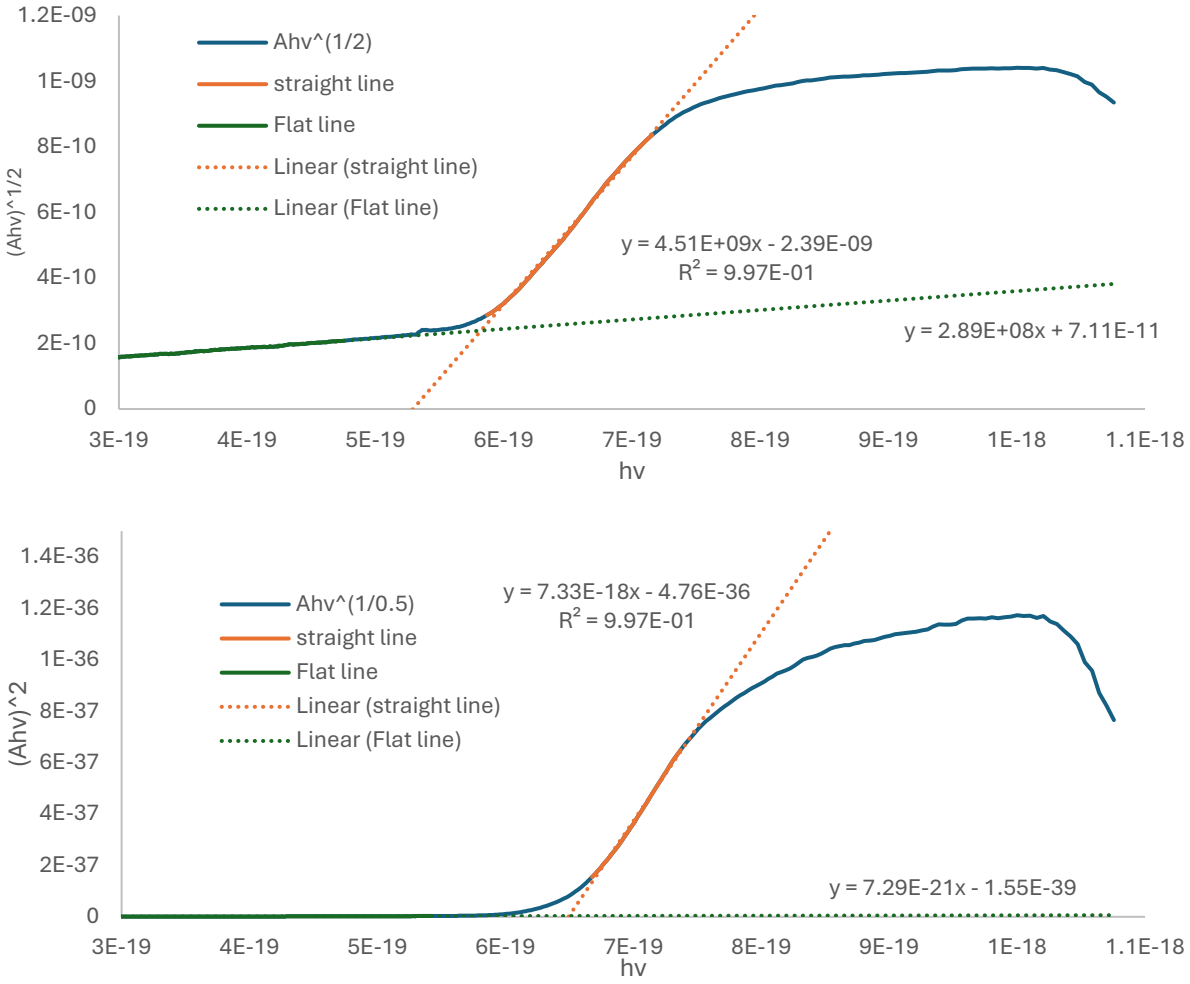

Figure S18. Tauc plots for [Ti(OAd)$_4$] in the solids-state; top, indirect onset; bottom, direct onset. Flat line is extrapolation of baseline.

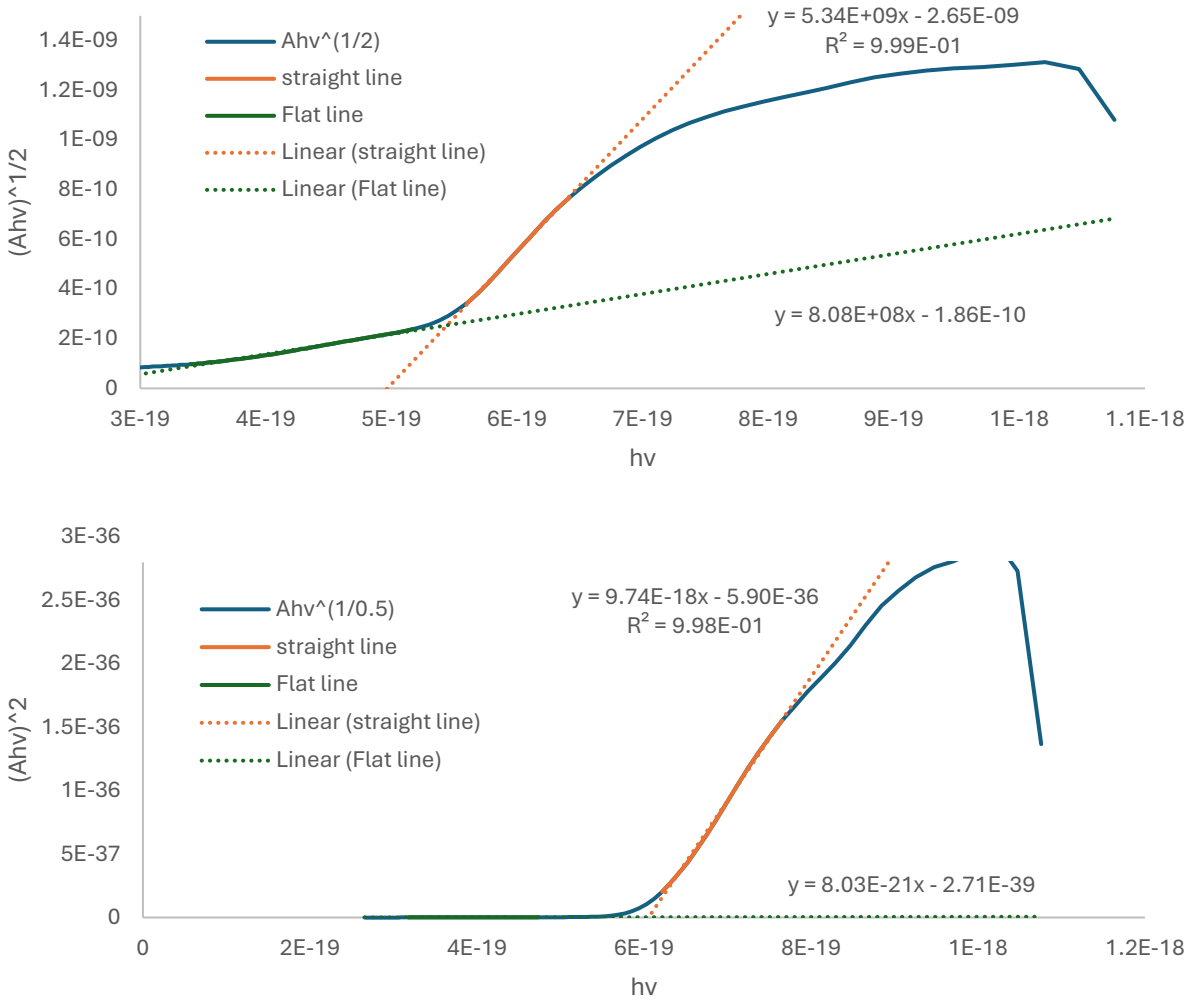

Figure S19. Tauc plots for $[Ti(OMe)_4]_4$ in the solid-state; top, indirect onset; bottom, direct onset. Flat line is extrapolation of baseline.

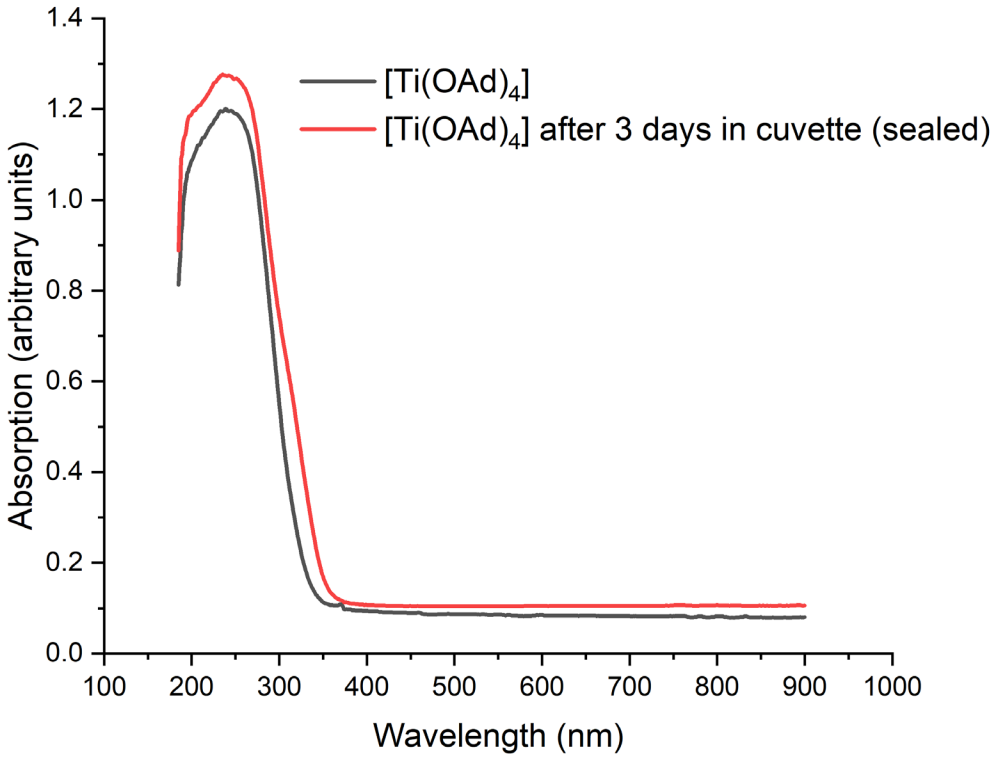

Figure S20. Diffuse reflectance UV/visible absorption spectrum of $[Ti(OAd)_4]$ in a vacuum grease sealed quartz cuvette over time. Initial spectrum taken immediately after removing from glovebox.

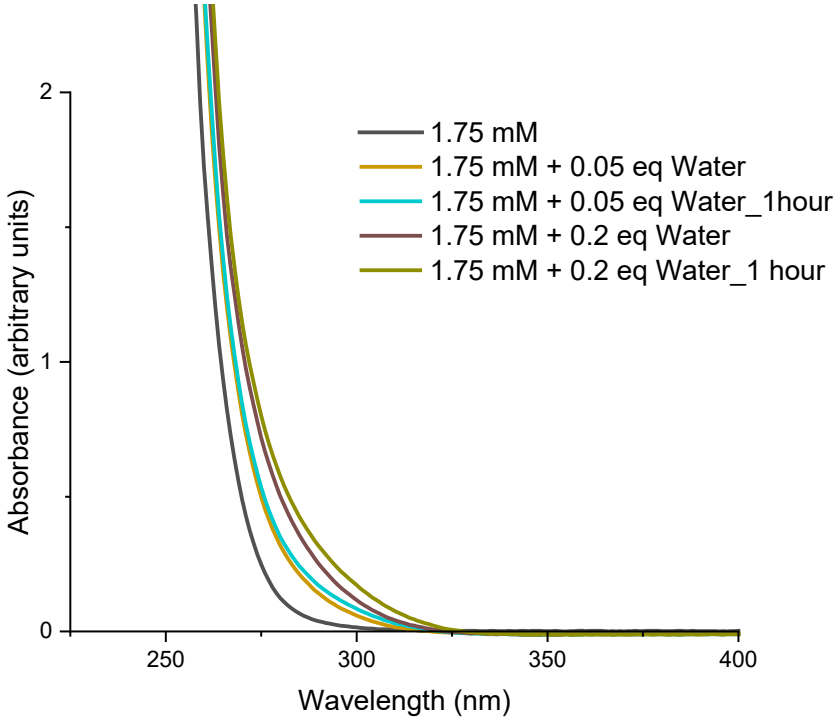

Figure S21. UV spectra of $[Ti(O^iPr)_4]$ with 0.05 or 0.2 equivalents of water added. The UV spectra of $[Ti(O^iPr)_4]$ red shifts on introduction of small amounts of moisture, indicating that hydrolysis and condensation reactions create larger clusters that absorb at higher wavelengths.

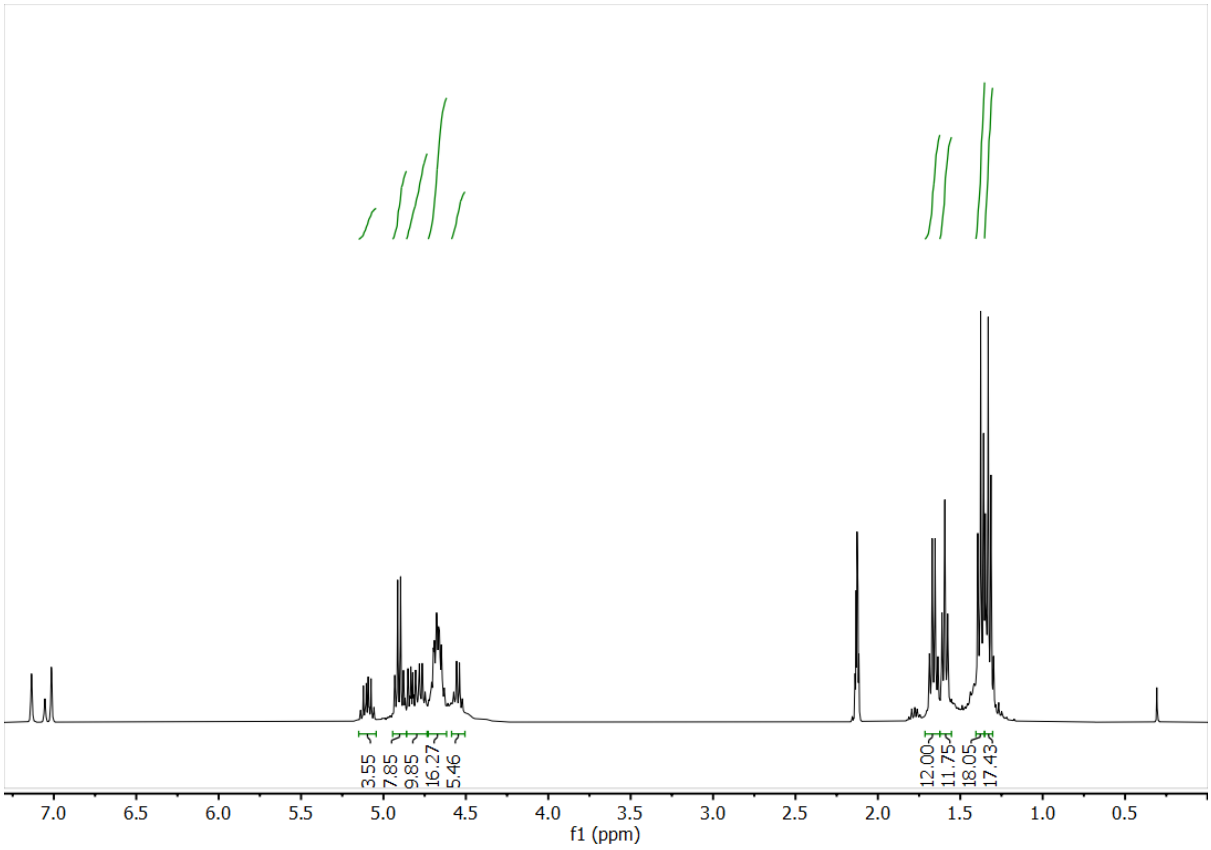

Figure S22. ^{1}H NMR spectrum of **Ti$_7$** in d$_8$-toluene.

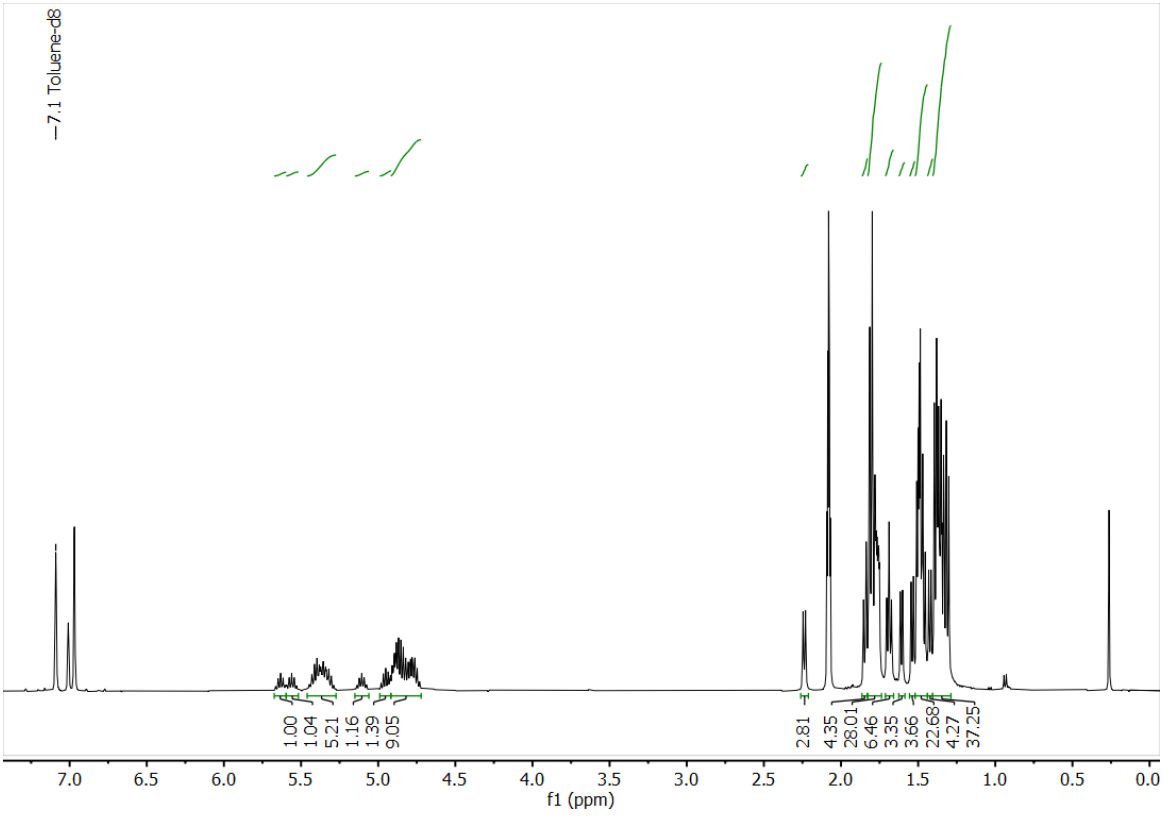

Figure S23. ^{1}H NMR spectrum of **Ti$_{11}$** in d$_8$-toluene. Consistent with the expected 18 O^{i}Pr groups.

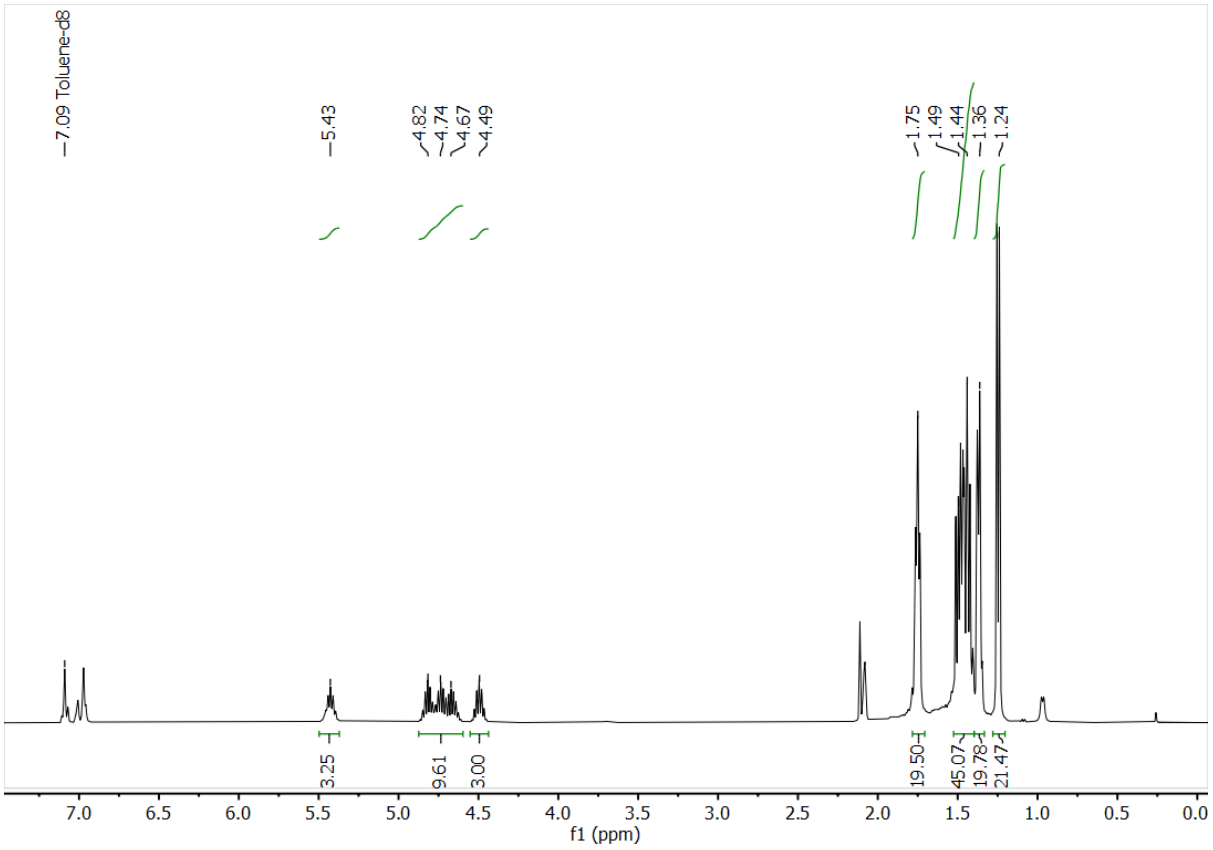

Figure S24. ^{1}H NMR spectrum of **Ti$_{12}$** in d$_8$-toluene. Consistent with the expected 16 O^{i}Pr groups.

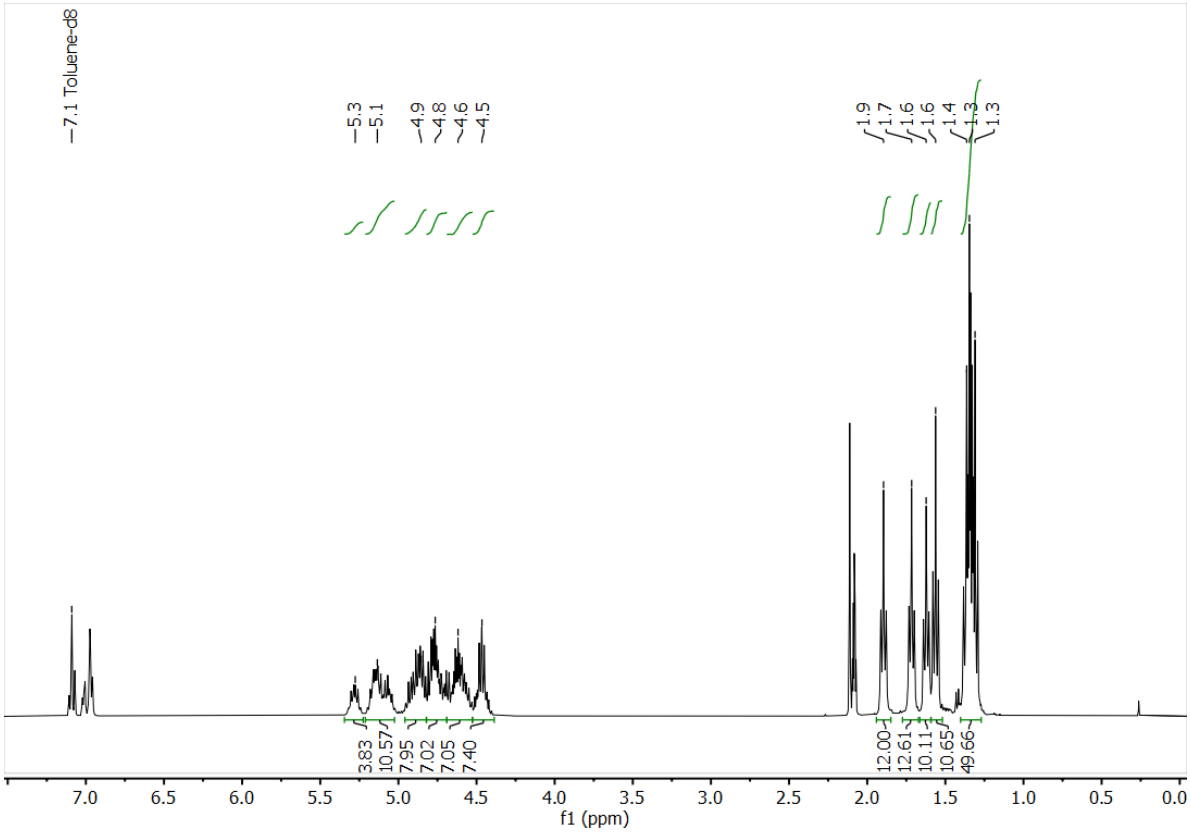

Figure S25. ^{1}H NMR spectrum of **Ti$_{16}$** in d$_8$-toluene

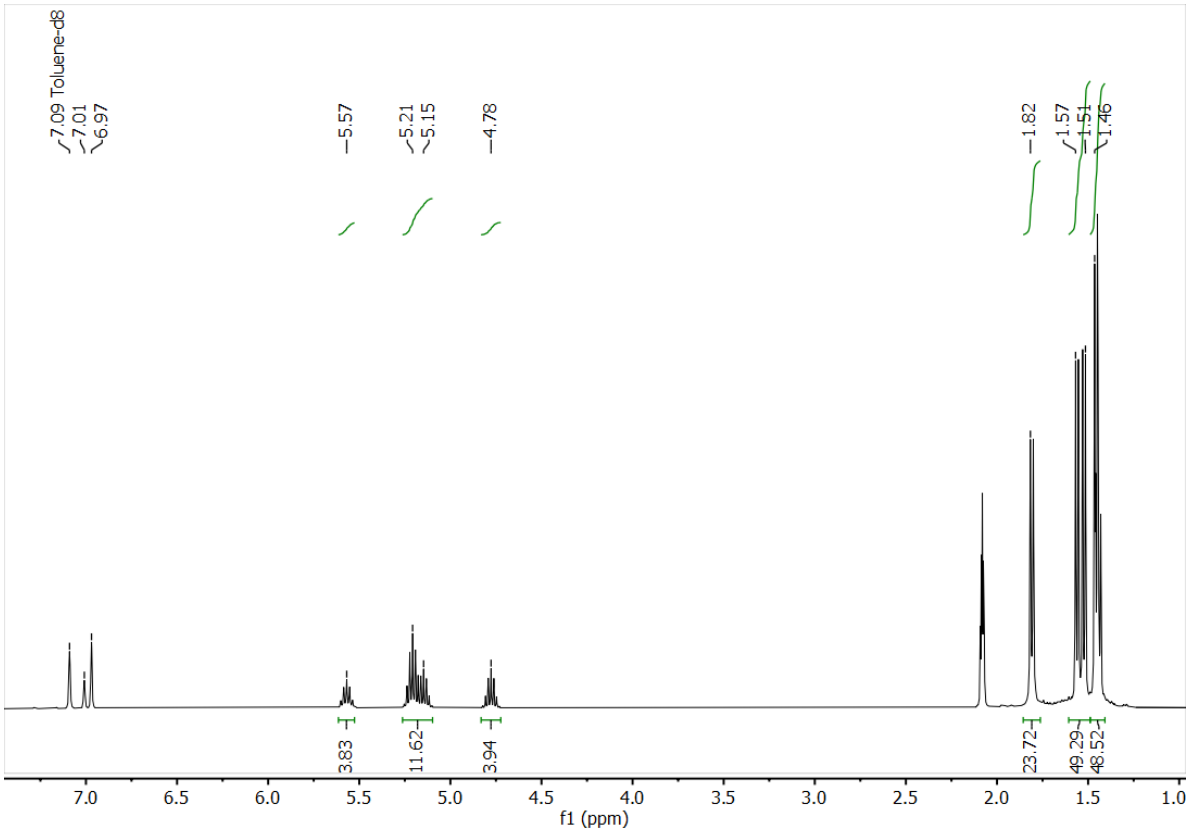

Figure S26. ^{1}H NMR spectrum of **Ti_{17}** in d_8-toluene

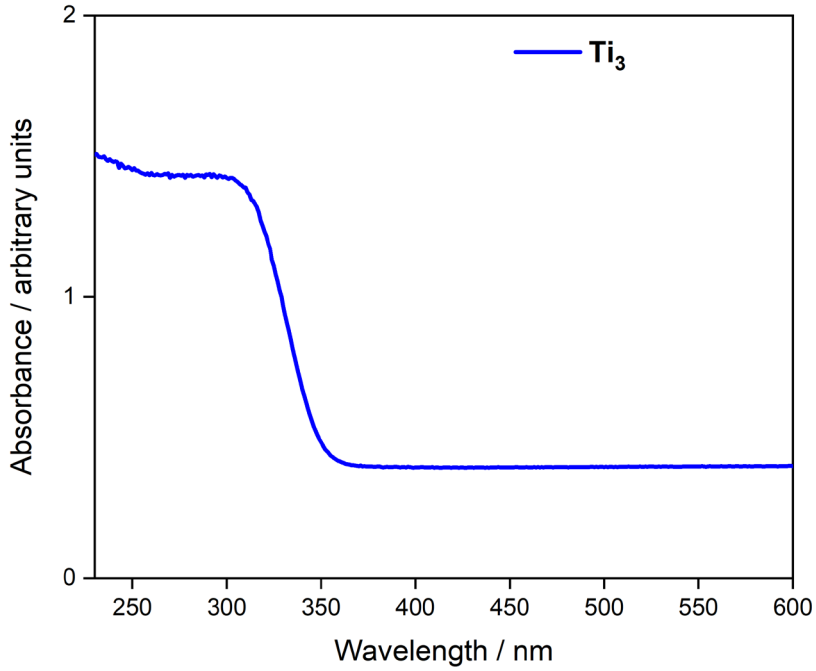

Figure S27. DRS UV/vis spectrum of **Ti_3**. Note the baseline shift from zero is due to the use of an air-sensitive sample holder, which results is some light escaping from the sides of the holder.

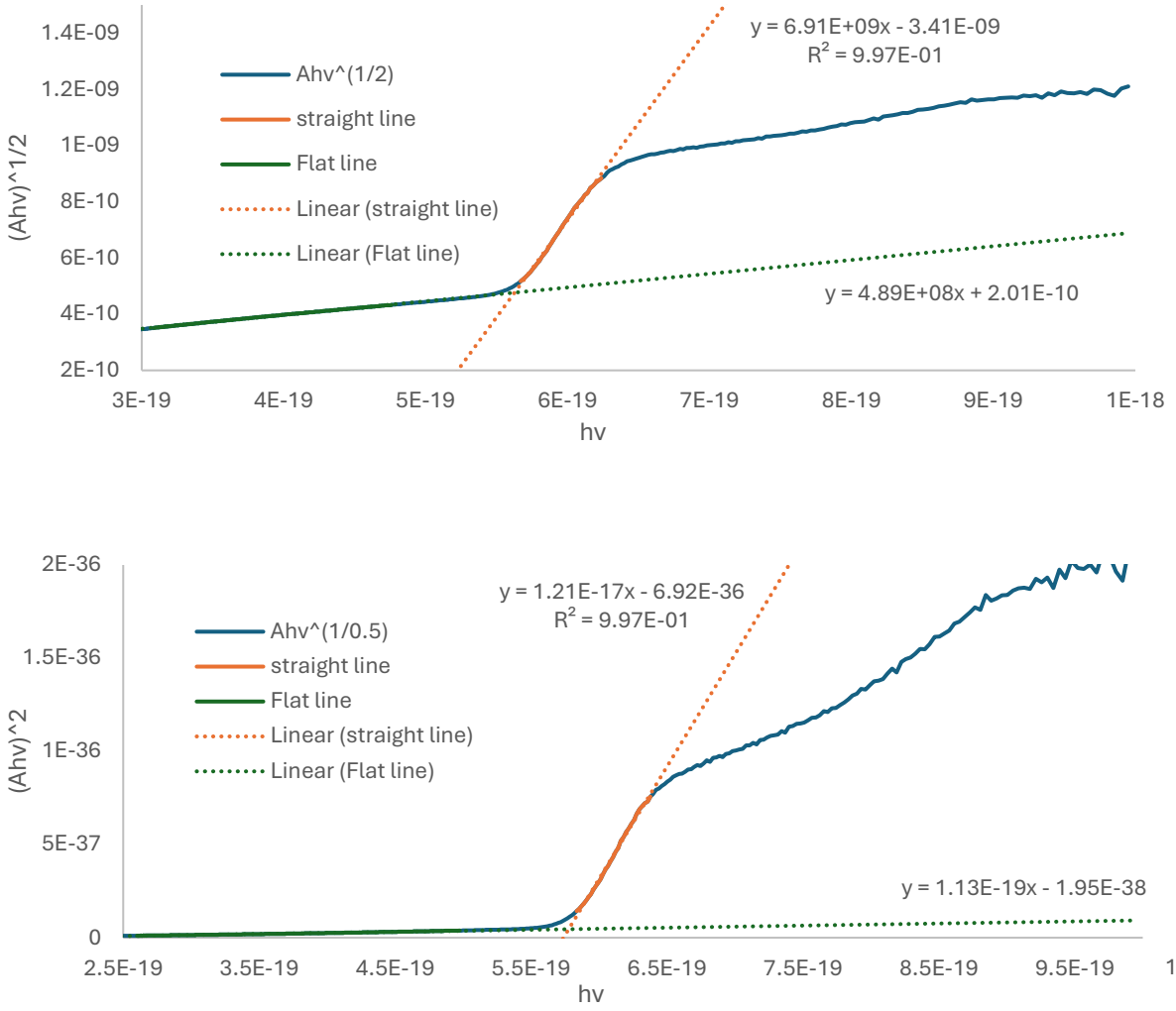

Figure S28. Tauc plots for **Ti_3** in the solid-state; top, indirect onset; bottom, direct onset. Flat line is extrapolation of baseline.

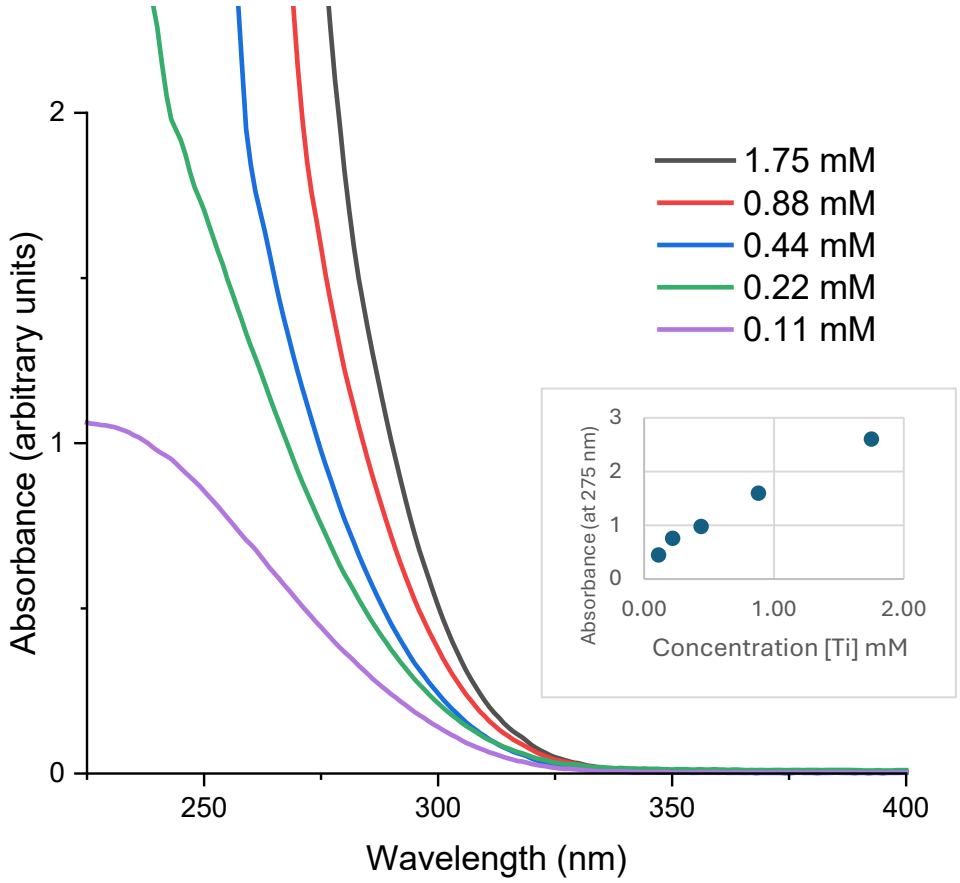

Figure S29. UV spectra of crystals of **Ti_3** dissolved in pentane at various concentrations (concentration calculated per Ti). **Ti_3** is known to form an equilibrium in solution between $[Ti(OR)_4]$, **Ti_3** and small quantities of larger Ti-oxo clusters such as **Ti_{11}.** Indirect onset at [Ti] = 1.75 mM calculated at 3.68 eV, direct onset calculated at 4.45 eV.

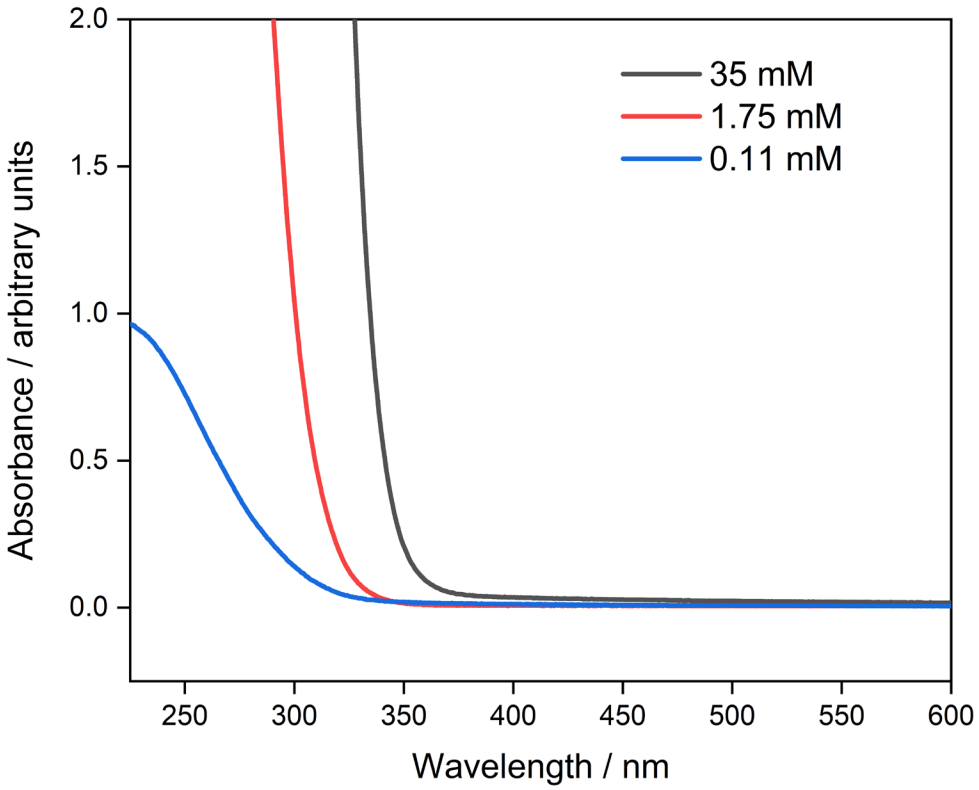

Figure S30. UV spectra of crystals of **Ti_7** dissolved in pentane at various concentrations (concentration calculated per Ti).

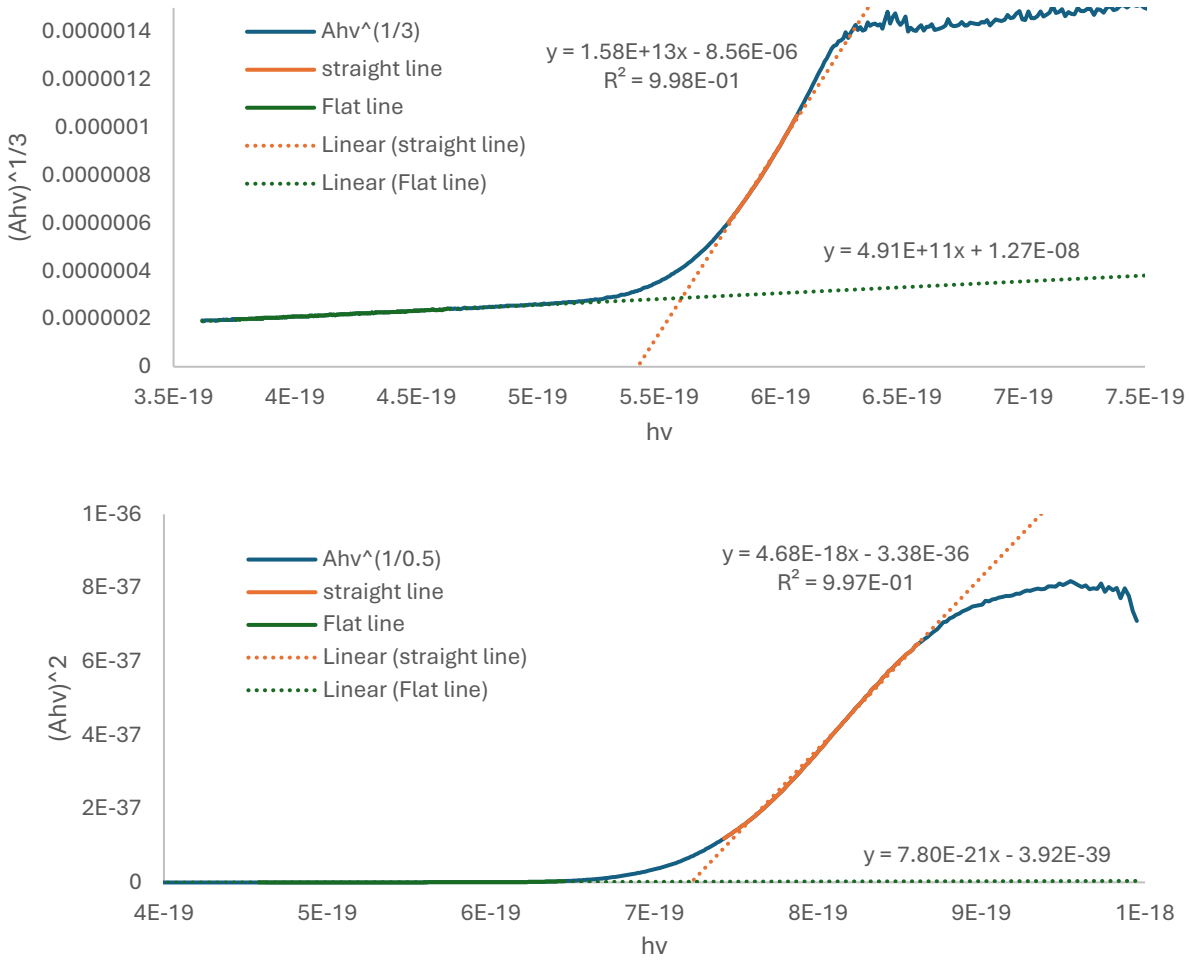

Figure S31. Tauc plots **Ti_7** in solution, top [Ti] = 35 mM n = 3, bottom [Ti] = 0.11 mM n = 0.5. Flat line is extrapolation of baseline.

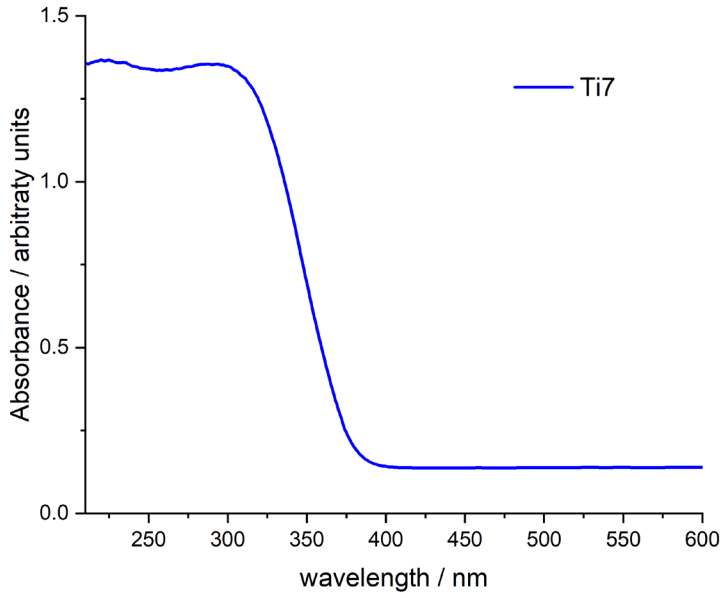

Figure S32. Diffuse reflectance UV/visible spectrum of **Ti_7**

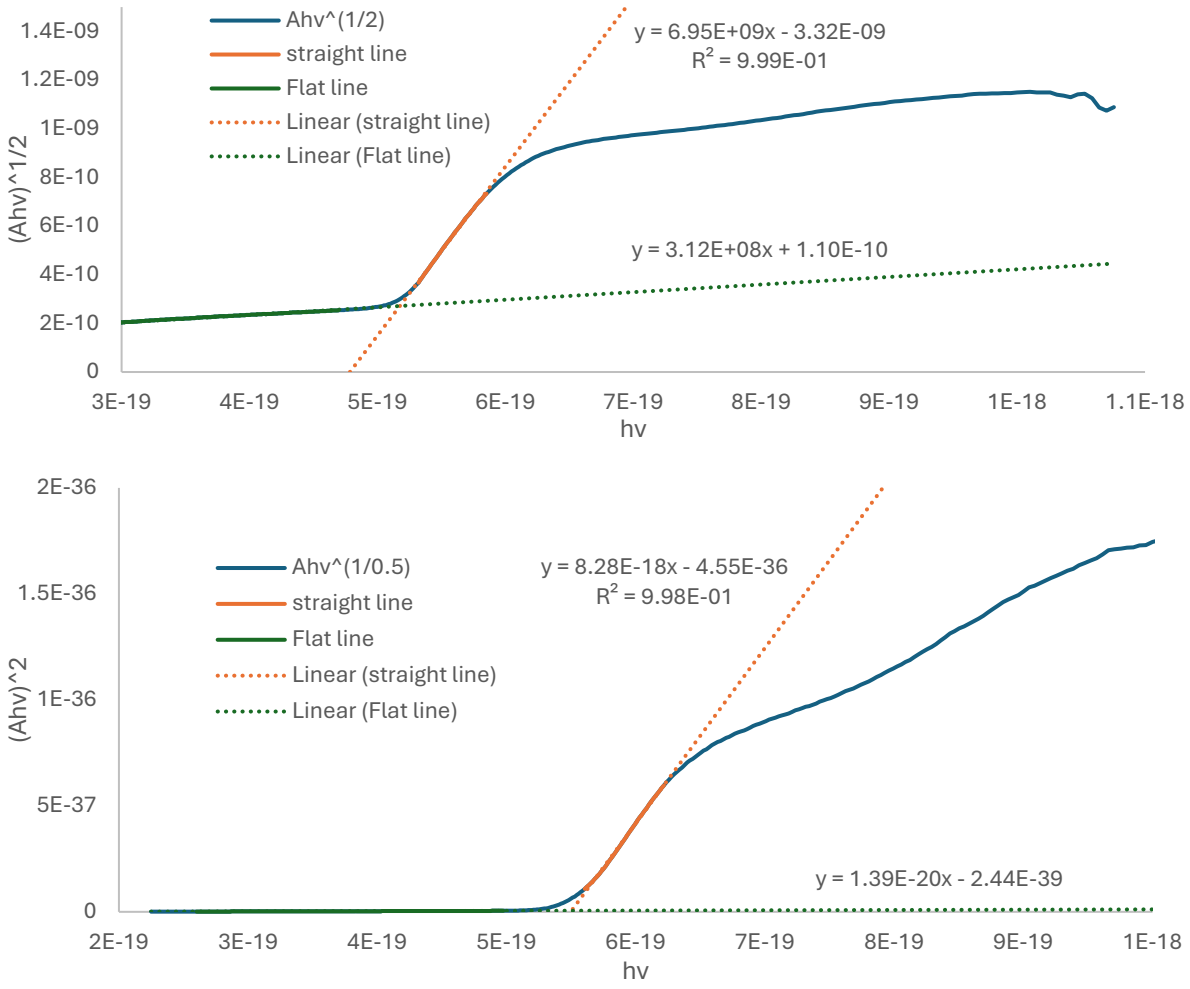

Figure S33. Tauc plots for **Ti_7** in the solid-state, top, indirect onset; bottom, direct onset. Flat line is extrapolation of baseline.

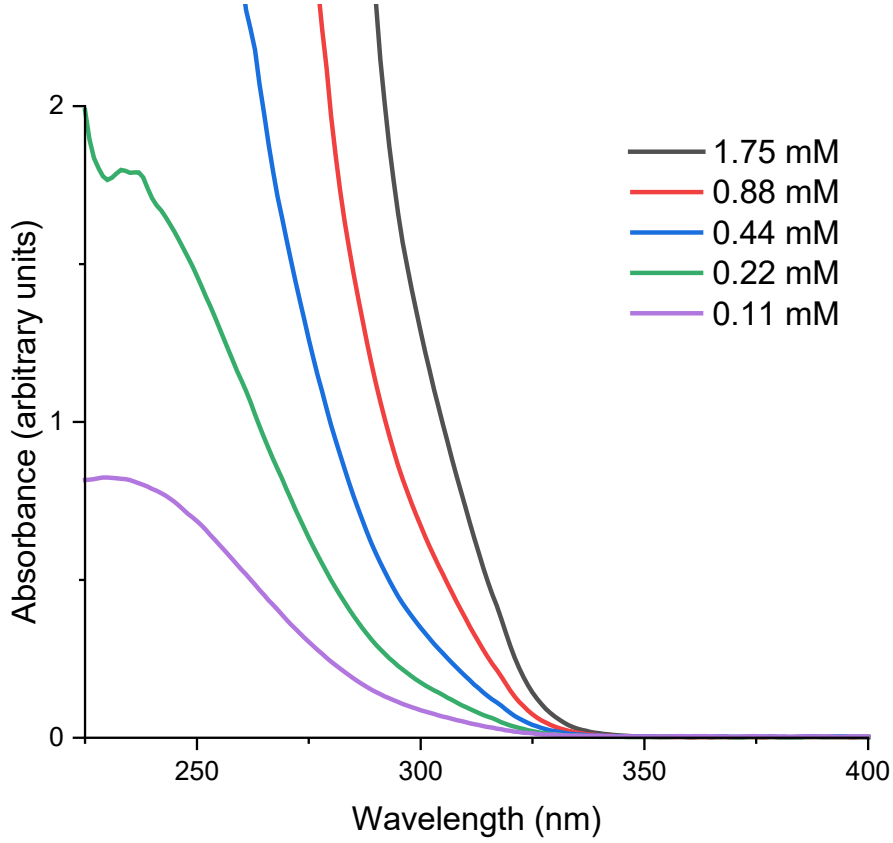

Figure S34. UV spectra of $Ti_{11}O_{13}(O^iPr)_{18}$ dissolved in pentane at various concentrations (concentration calculated per Ti).

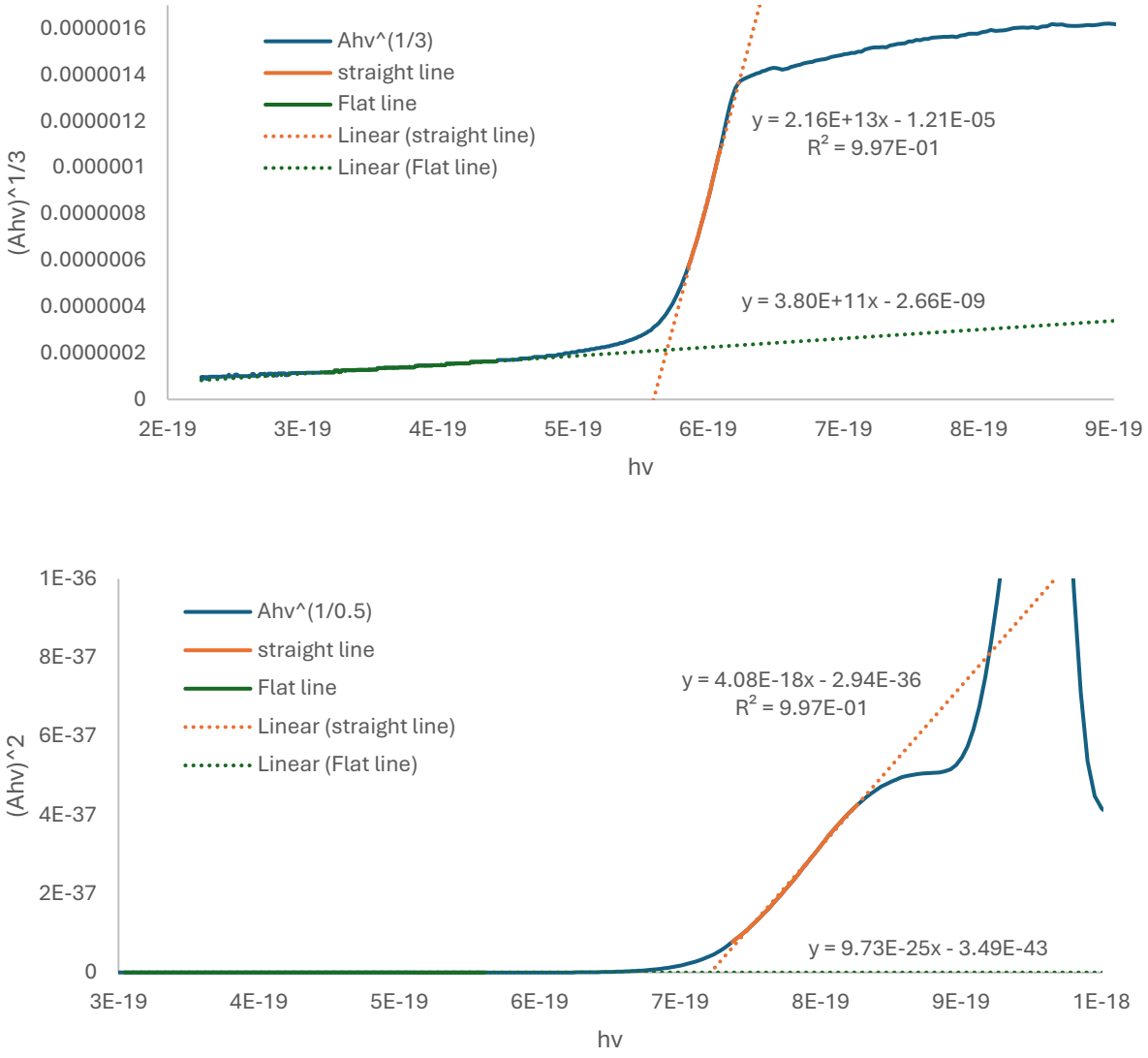

Figure S35. Tauc plots for **Ti_{11}** in solution, top [Ti] = 35 mM n = 3, bottom [Ti] = 0.11 mM n = 0.5. Flat line is extrapolation of baseline.

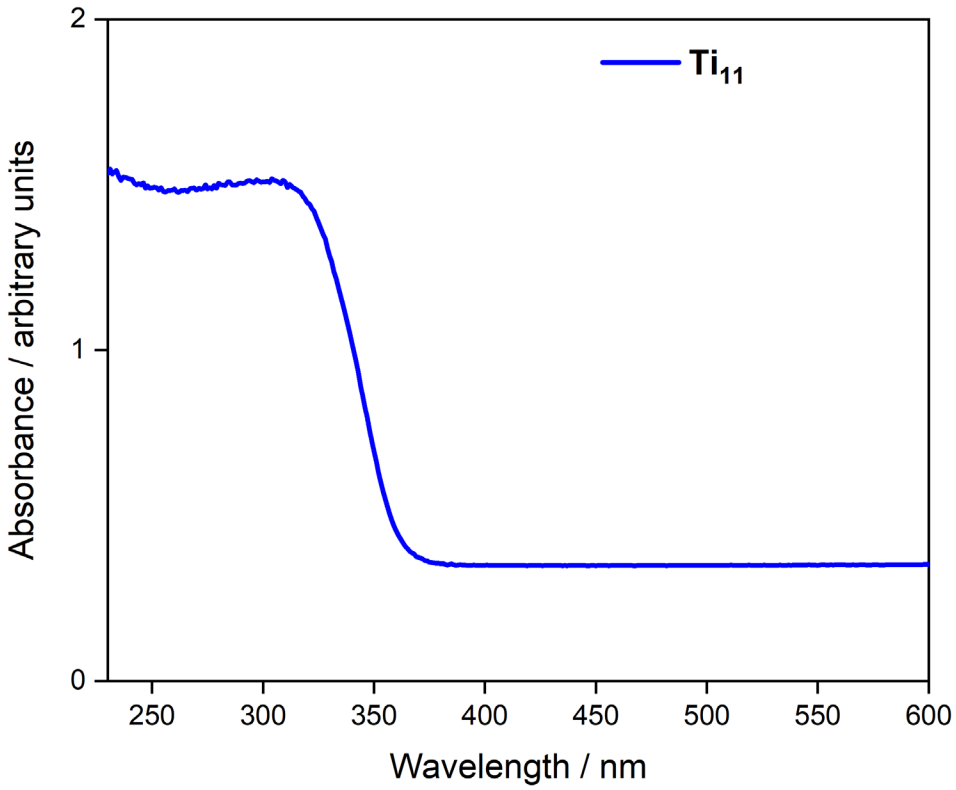

Figure S36. Diffuse reflectance UV/visible spectrum of **Ti_{11}**

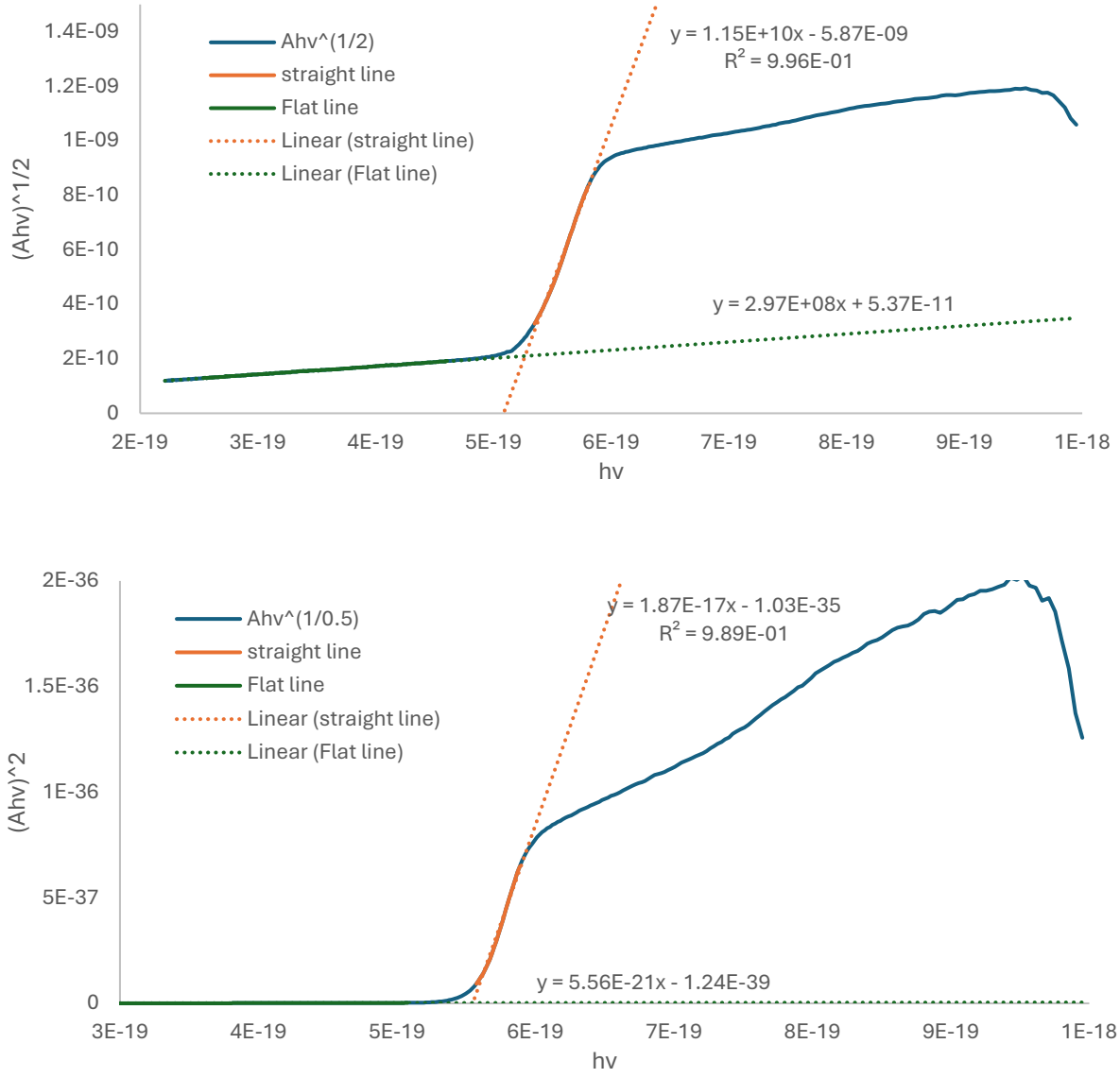

Figure S37. Tauc plots for **Ti_{11}** in the solid-state, top, indirect onset; bottom, direct onset. Flat line is extrapolation of baseline.

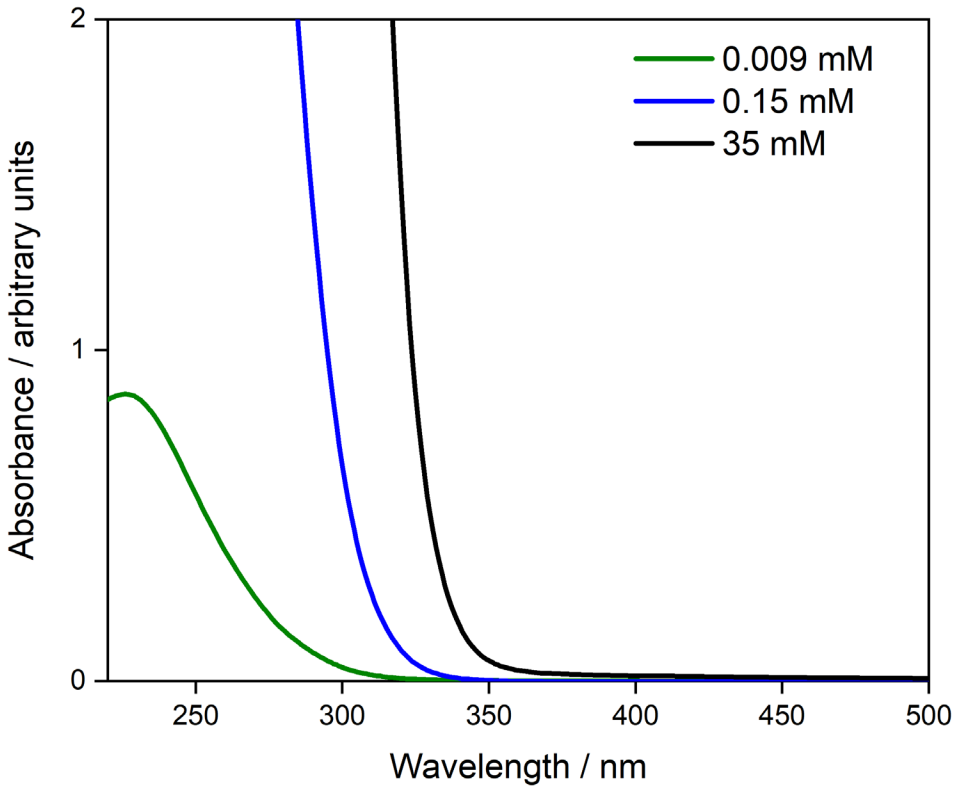

Figure S38. UV spectra of **Ti_{12}** dissolved in pentane at various concentrations (concentration calculated per Ti).

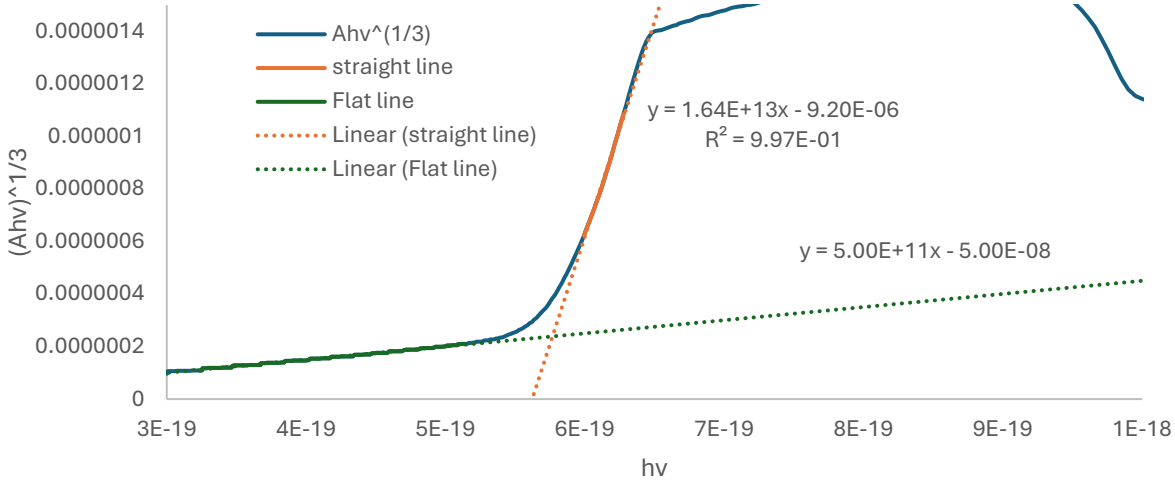

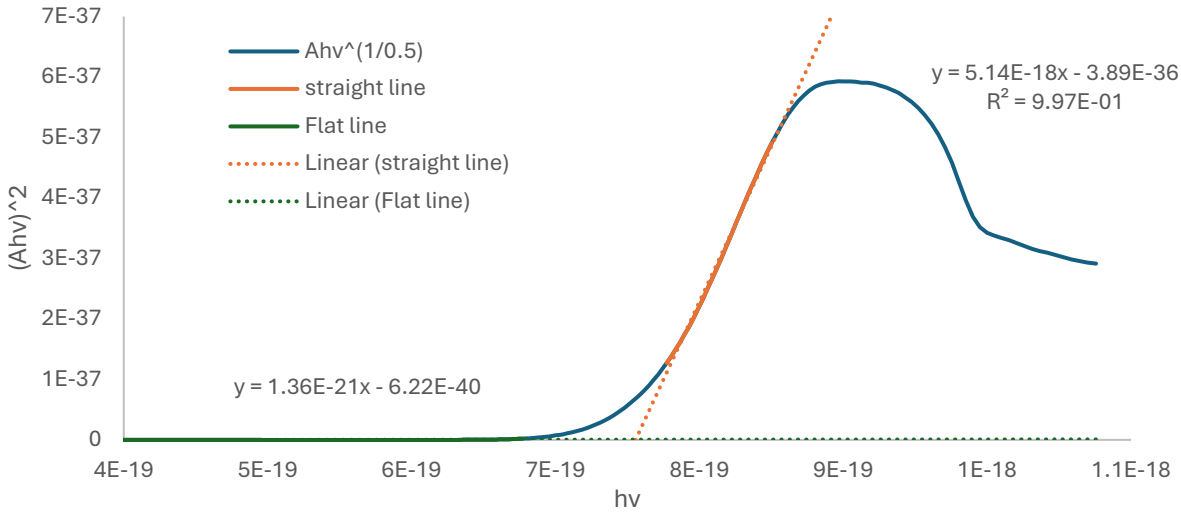

Figure S39. Tauc plots for **Ti_{12}** in solution, top [Ti] = 35 mM n = 3, bottom [Ti] = 0.11 mM n = 0.5. Flat line is extrapolation of baseline.

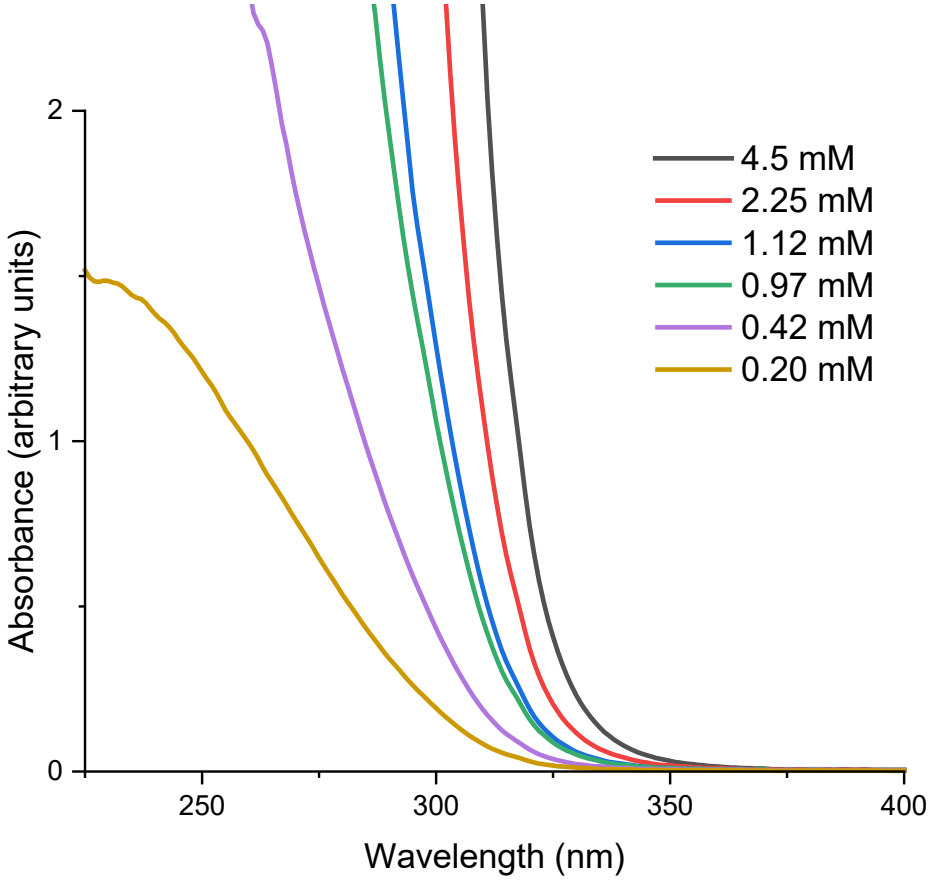

Figure S40. UV spectra of **Ti_{16}** dissolved in pentane at various concentrations (concentration calculated per Ti).

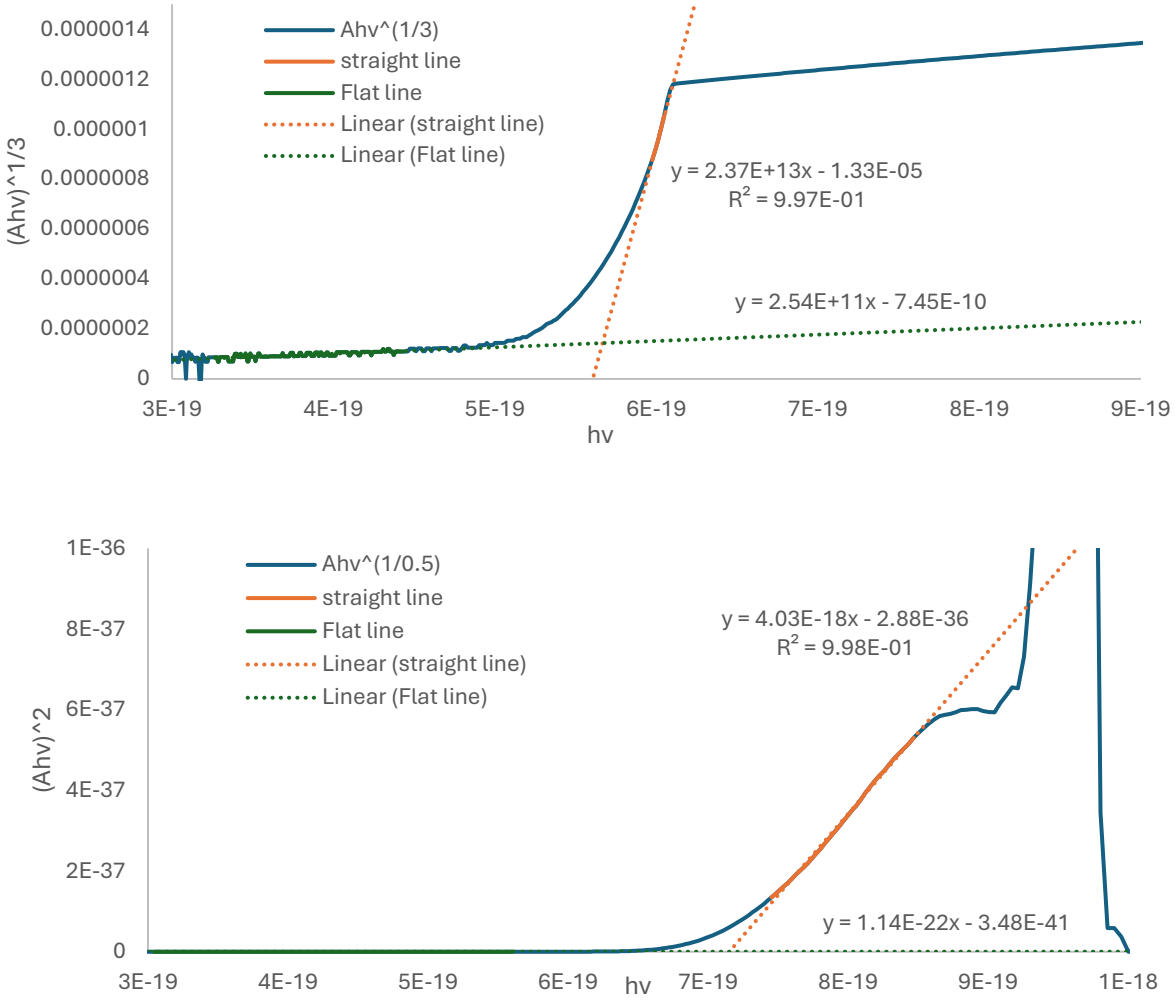

Figure S41. Tauc plots for **Ti_{16}** in solution; top [Ti] = 35 mM n = 3, bottom [Ti] = 0.11 mM n = 0.5. Flat line is extrapolation of baseline.

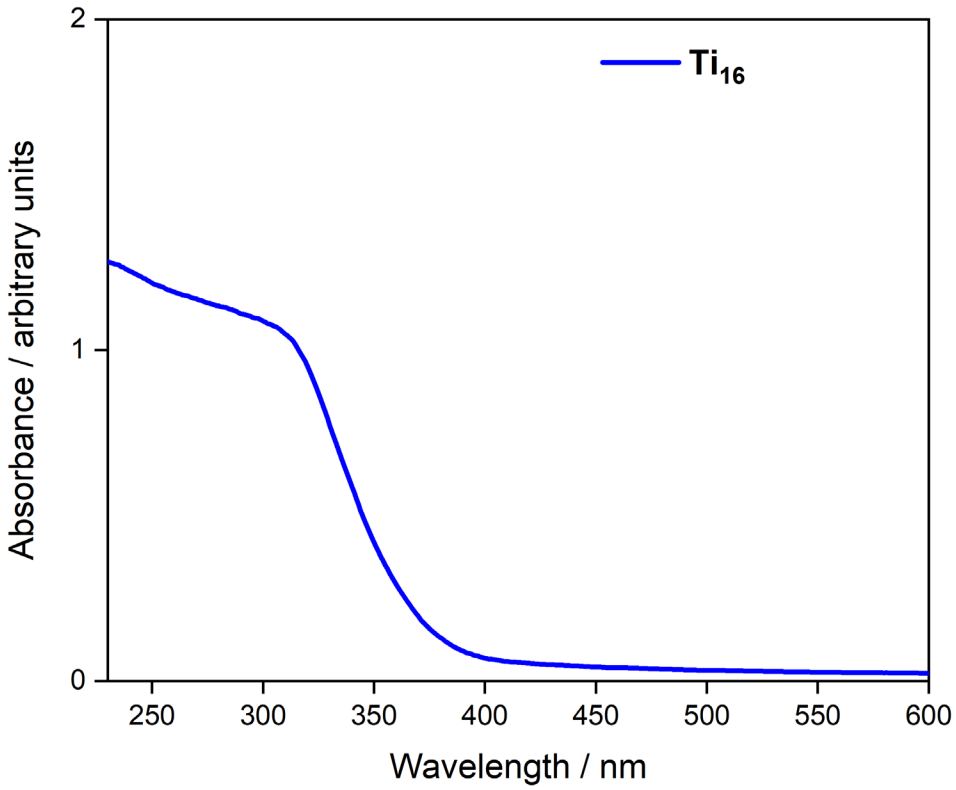

Figure S42. Diffuse reflectance UV/visible spectrum of **Ti_{16}**

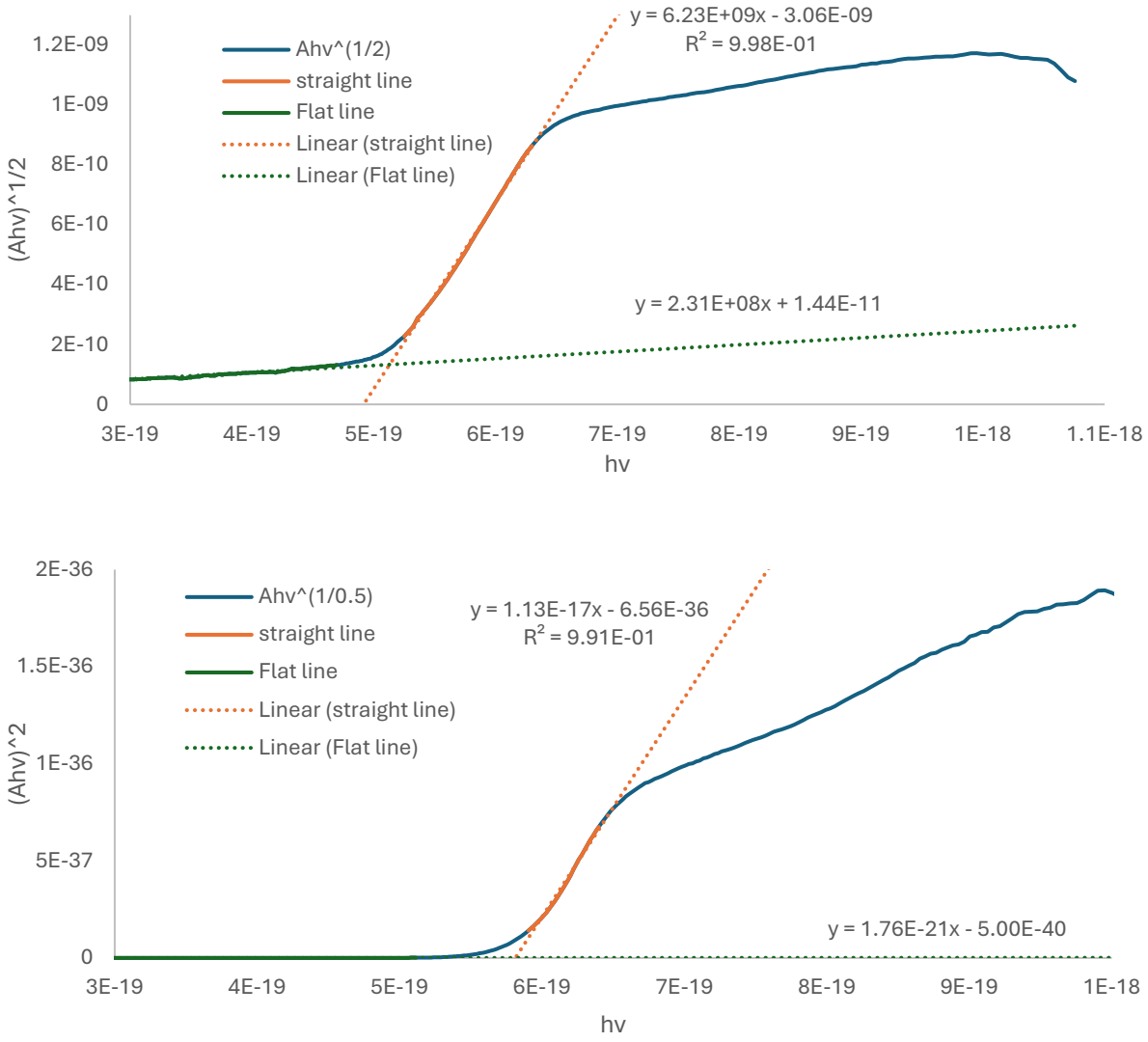

Figure S43. Tauc plots for **Ti_{16}** in the solid-state; top, indirect onset; bottom, direct onset. Flat line is extrapolation of baseline.

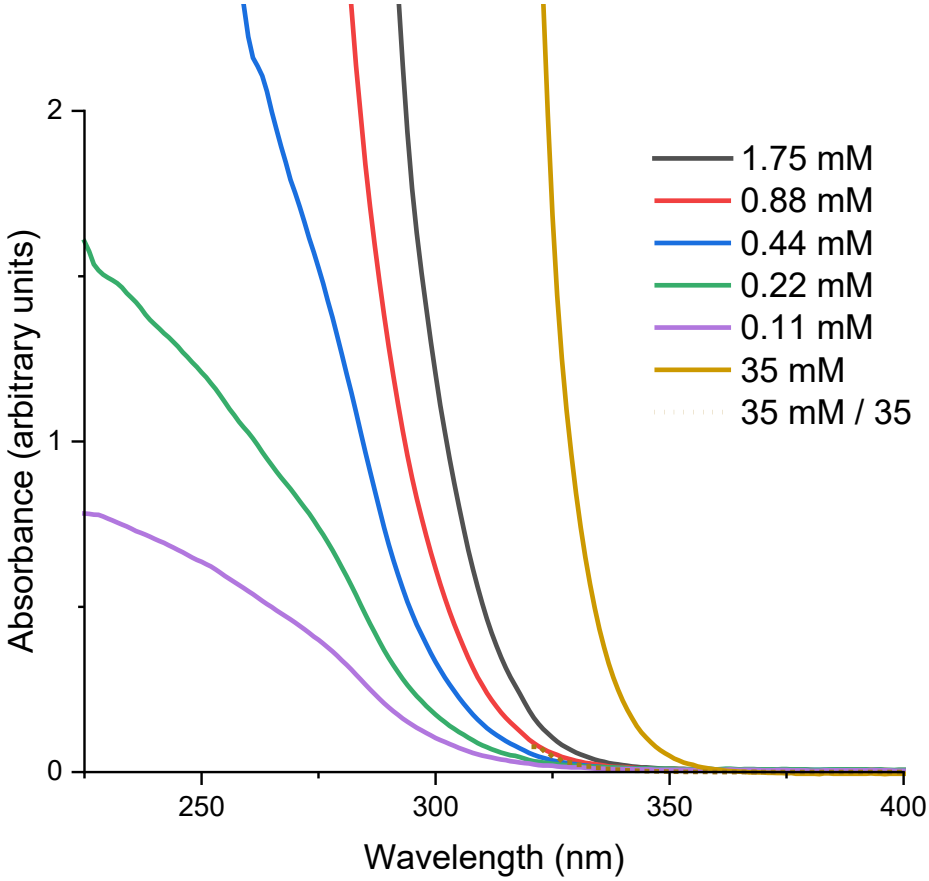

Figure S44. UV spectra of $\mathbf{Ti_{17}}$ dissolved in pentane at various concentrations (concentration calculated per Ti).

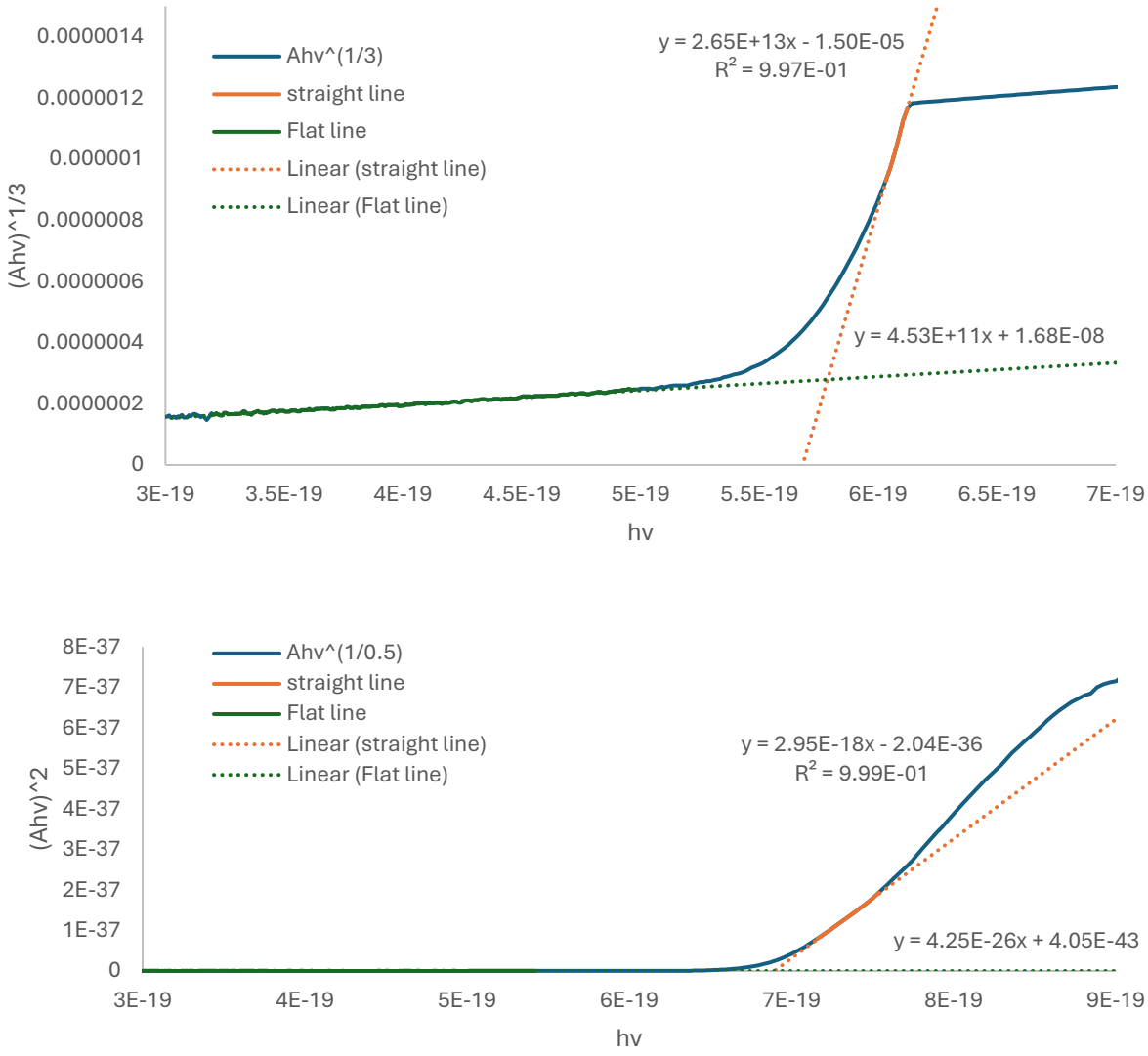

Figure S45. Tauc plots for **Ti_{17}** in solution; top [Ti] = 35 mM n = 3, bottom [Ti] = 0.11 mM n = 0.5. Flat line is extrapolation of baseline.

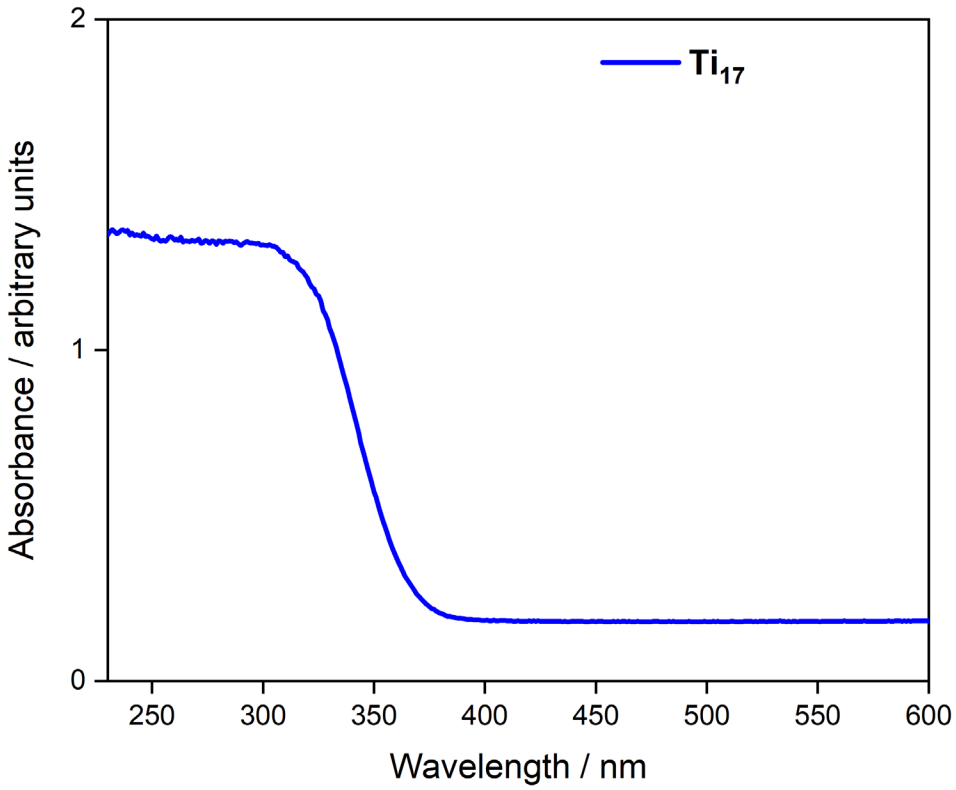

Figure S46. Diffuse reflectance UV/visible spectrum of **Ti_{17}**

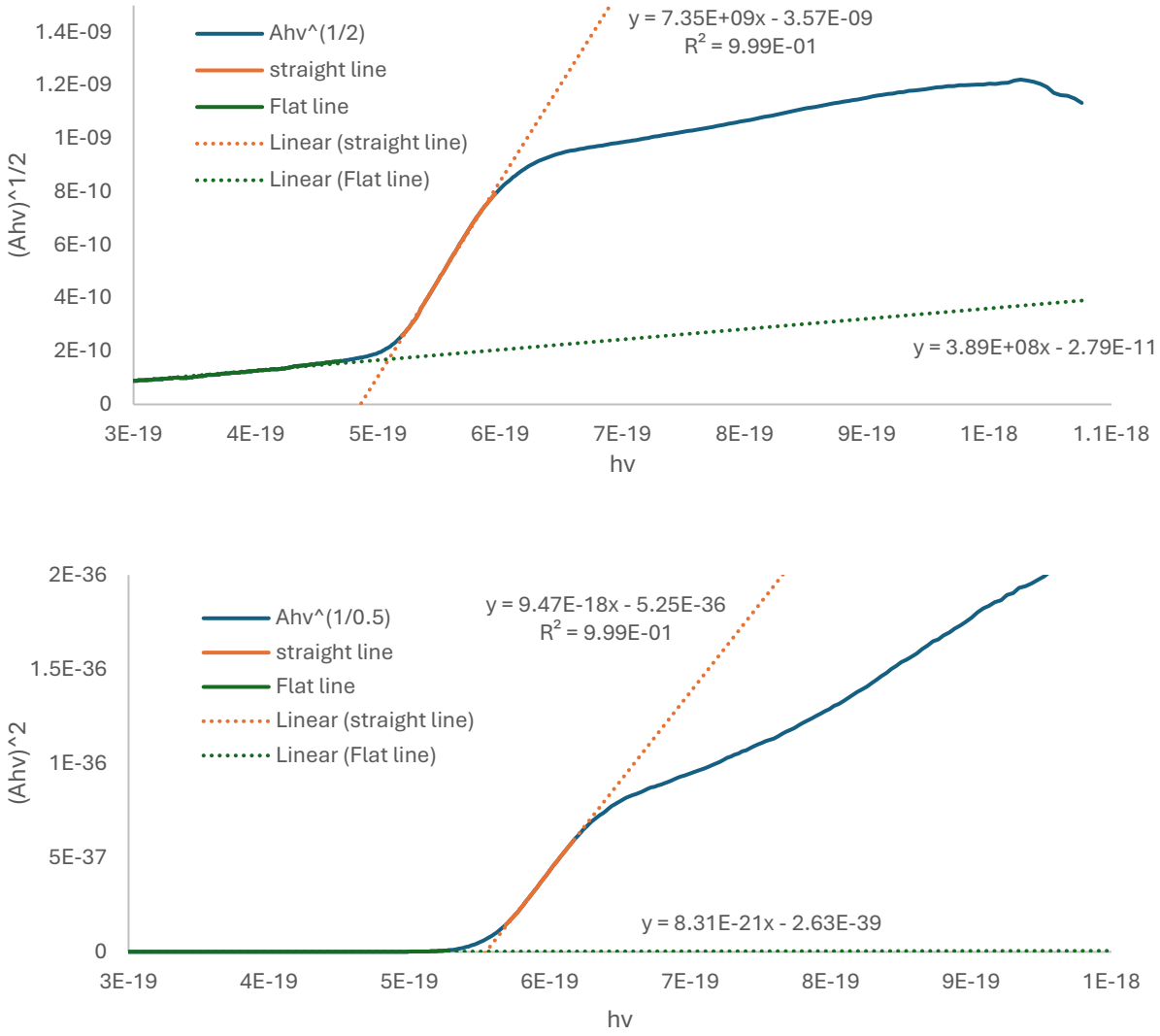

Figure S47. Tauc plots for **Ti_{17}** in the solid-state; top, indirect onset; bottom, direct onset. Flat line is extrapolation of baseline.

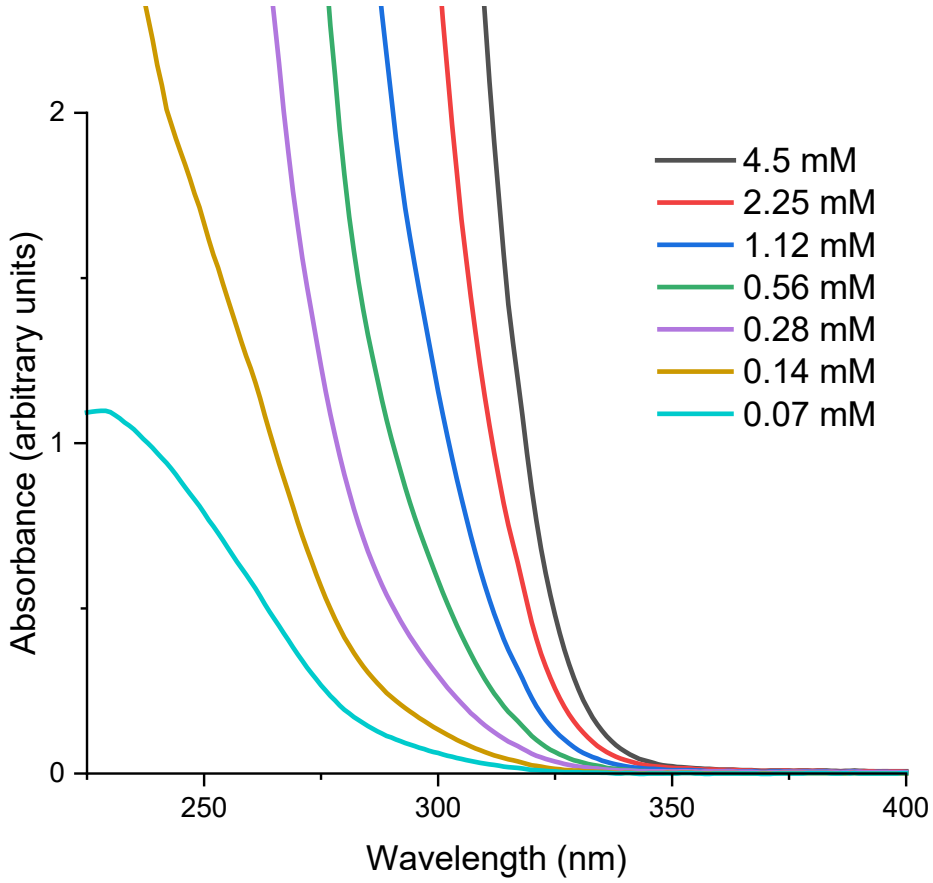

Figure S48. UV spectra of $\mathbf{Ti_{18}}$ dissolved in pentane at various concentrations (concentration calculated per Ti).

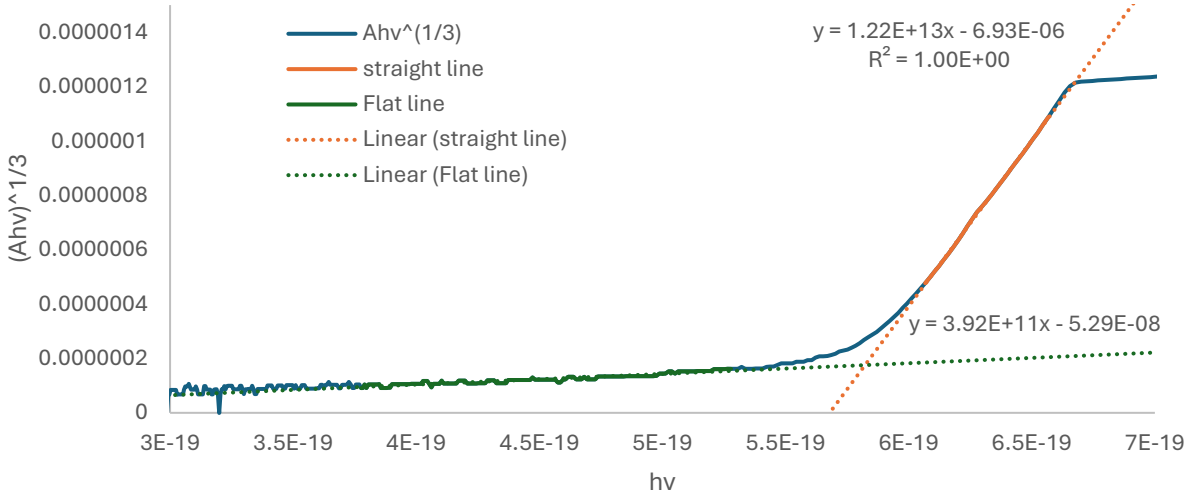

Figure S49. Tauc plot for **Ti_{18}** in solution; [Ti] = 2.25 mM, n = 3. Flat line is extrapolation of baseline.

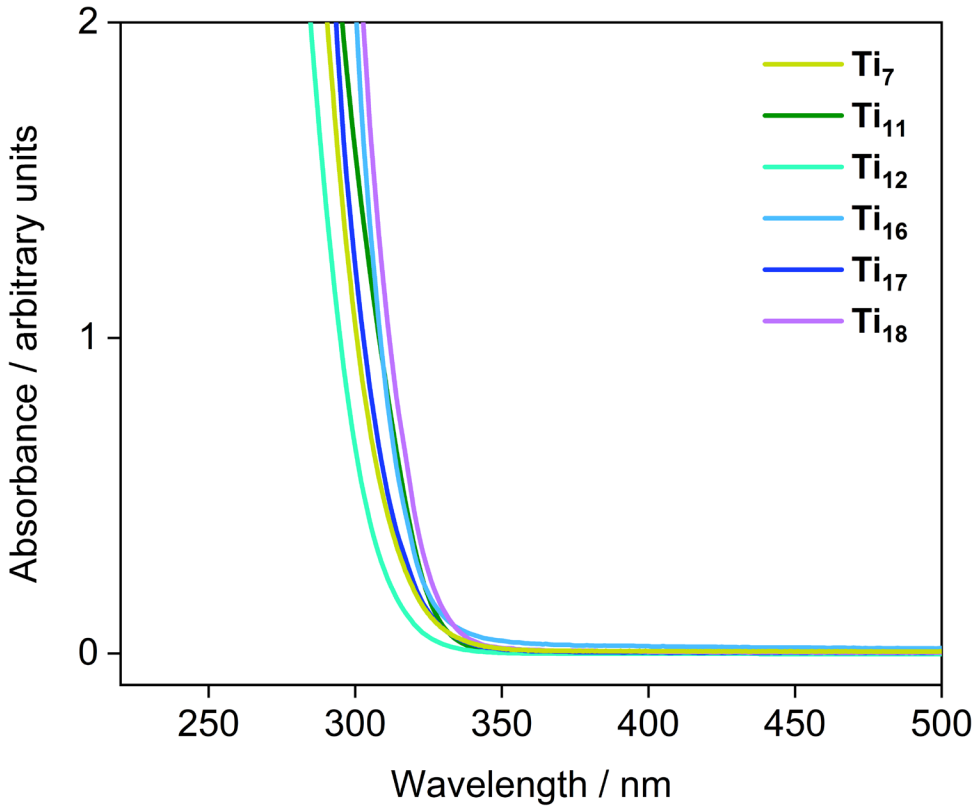

Figure S50. Solution ([Ti] = 1.75 mM) absorption spectra of titanium-oxo-alkoxides.

Table S2. Summary of absorption onsets of Ti(-oxo)-alkoxides. *In equilibria with other species. [#]2.25 mM. Values in bold are considered most reliable. [%]monomer dominant at <10 mM,[16] dimer may be present at 35 mM. †trimer dominant at 35 mM, dimer and monomer possible at lower concentrations.

No Ti atoms	UV data	**DRS (direct)**	DRS (indirect)	**[Ti] = 35 mM (indirect)**	[Ti] = 1.75 mM (indirect)	[Ti] = 0.1 mM (direct)
1	$[Ti(O^tBu)_4]$			**4.16**	4.26	4.93
1 / 2[%]	$[Ti(O^iPr)_4]$			**3.96**[%]	4.33	4.91
1	$[Ti(OAd)_4]$	**4.14**	3.57		4.26	4.79
2 / 3†	$[Ti(OEt)_4]_n$			**3.57†**	3.73	4.39
3	**Ti_3**	**3.61**	3.51		3.68*	4.45*
4	$[Ti(OMe)_4]_4$	**3.78**	3.4			
7	**Ti_7**	**3.44**	3.23	**3.49**	3.65	4.51
11	**Ti_{11}**	**3.5**	3.41	**3.55**	3.61	4.5
12	**Ti_{12}**			**3.6**	3.75	4.72
16	**Ti_{16}**	**3.55**	3.17	**3.54**	3.71	4.46
17	**Ti_{17}**	**3.5**	3.33	**3.61**	3.62	4.30
18	**Ti_{18}**				3.64[#]	
Bulk	**Anatase**	**3.32**	3.14			
Bulk	**Rutile**	**3.07**	2.93			

Table S3. Sizes of the Ti – O core of the Ti-oxo-alkoxides used in this work.

Cluster	**Core**	**Core Size[a] / nm**
$[Ti(OAd)_4]$	TiO_4	2x Ti-O distance = 0.35
Ti_3	Ti_3O_{11}	0.53 (0.24)
$[\{Ti(OMe)_4\}_4]$	Ti_4O_{16}	0.87 (0.25)
Ti_7	Ti_7O_{24}	0.91 (0.49)
Ti_{11}	$Ti_{11}O_{31}$	0.98 (0.80)
Ti_{12}	$Ti_{12}O_{32}$	0.98 (0.80)
Ti_{16}	$Ti_{16}O_{48}$	1.30 (1.11)
Ti_{17}	$Ti_{17}O_{44}$	1.17 (1.06)
Ti_{18}	$Ti_{18}O_{45}$	1.17 (1.05)

a – Core size is estimated from the single crystal solid-state structures using the largest O – O distance that passes approximately through the centre of the molecule. As these are all pseudo-spherical structures (**Ti_3** and **$[\{Ti(OMe)_4\}_4]$** closer to planar), the shortest O – O (passing approximately through the centre of the molecule) distance is also given in brackets.

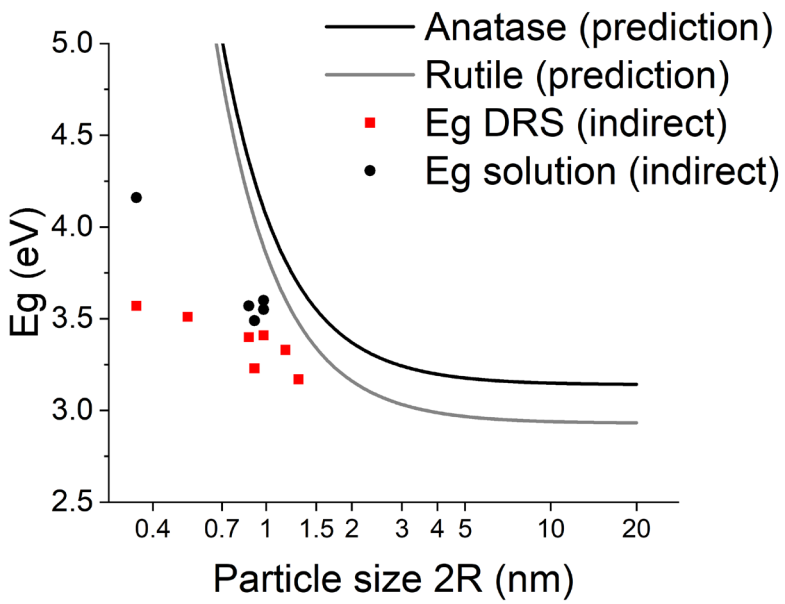

Figure S51. Absorption onsets of Ti-alkoxides and Ti-oxo-alkoxides in this study plotted against their maximum core dimension and in comparison, to the band gap prediction for TiO_2 particles based on quantum confinement effects using the effective mass approximation. Values from the Nosaka equation (similar to Brus equation), with a μ' value of 1.63 m_o and Eg(bulk) values derived from DRS measurements in this study.[19]

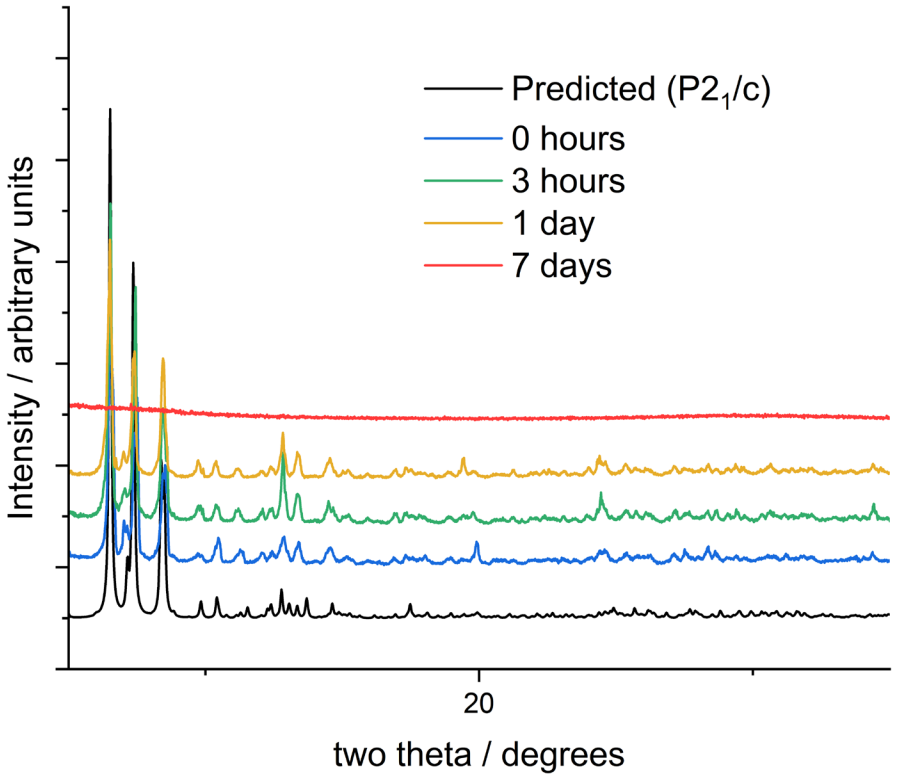

Figure S52. Powder X-ray diffraction patterns of microcrystalline **Ti_{16}** over time under air.

Table S4. Benchmarking the molecular orbital energies of the HOMO and LUMO and bandgap with different density functionals. All values are in atomic units.

Functionals	Clusters	HOMO	LUMO	Gap
PBE	Ti1	-0.2205	-0.0575	0.1630
	Ti2	-0.2130	-0.0755	0.1375
	Ti3	-0.2060	-0.0804	0.1256
	Ti7	-0.2060	-0.0873	0.1187
TPSSh	Ti1	-0.2389	-0.0338	0.2050
	Ti2	-0.2339	-0.0527	0.1812
	Ti3	-0.2288	-0.0586	0.1702
	Ti7	-0.2293	-0.0657	0.1636
PBE0	Ti1	-0.2718	-0.0158	0.2559
	Ti2	-0.2660	-0.0345	0.2315
	Ti3	-0.2611	-0.0416	0.2195
	Ti7	-0.2595	-0.0483	0.2112
CAMB3LYP	Ti1	-0.3267	0.0081	0.3348
	Ti2	-0.3181	-0.0015	0.3166
	Ti3	-0.3135	-0.0092	0.3043
	Ti7	-0.3113	-0.0172	0.2941

Table S5. Numerical results of HOMO and LUMO orbital energies for different sizes of titanium clusters calculated using PBE as the density functional in Fig. 5. Units are in atomic unit.

PBE	HOMO	LUMO	Gap
Ti1	-0.2205	-0.0575	0.1630
Ti2	-0.2130	-0.0755	0.1375
Ti3	-0.2060	-0.0804	0.1256
Ti4	-0.2060	-0.0858	0.1201
Ti7	-0.2060	-0.0873	0.1187
Ti11	-0.2096	-0.0936	0.1160
Ti12	-0.2171	-0.0987	0.1184
Ti16	-0.2093	-0.0987	0.1106
Ti17	-0.2189	-0.1054	0.1135

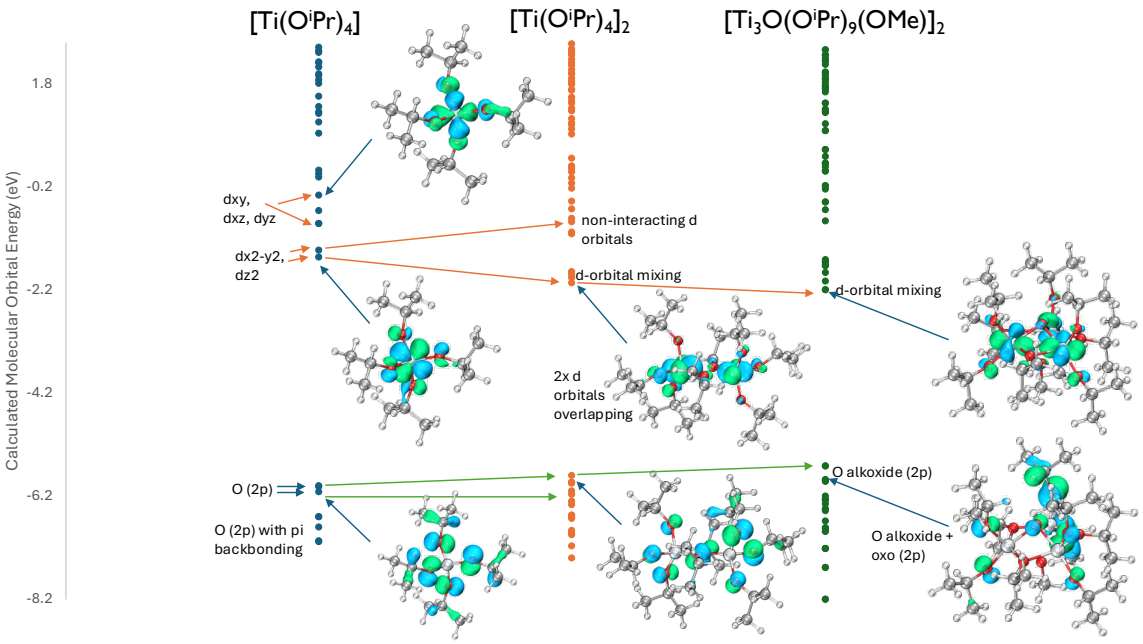

Figure S53. Energy positions (in Hartree) of frontier orbitals in [Ti(O^{i}Pr)$_4$], [{Ti(O^{i}Pr)$_4$}$_2$] and **Ti$_3$** calculated using PBE density functional. Figure shows the emergence of band-like electronic structure upon the increase of interacting atomic orbitals and the reduction of HOMO-LUMO energy gap. key d orbital based molecular orbitals highlighted in red and yellow dots, orbitals with oxo involvement shown with dark blue dots in **Ti$_3$**.

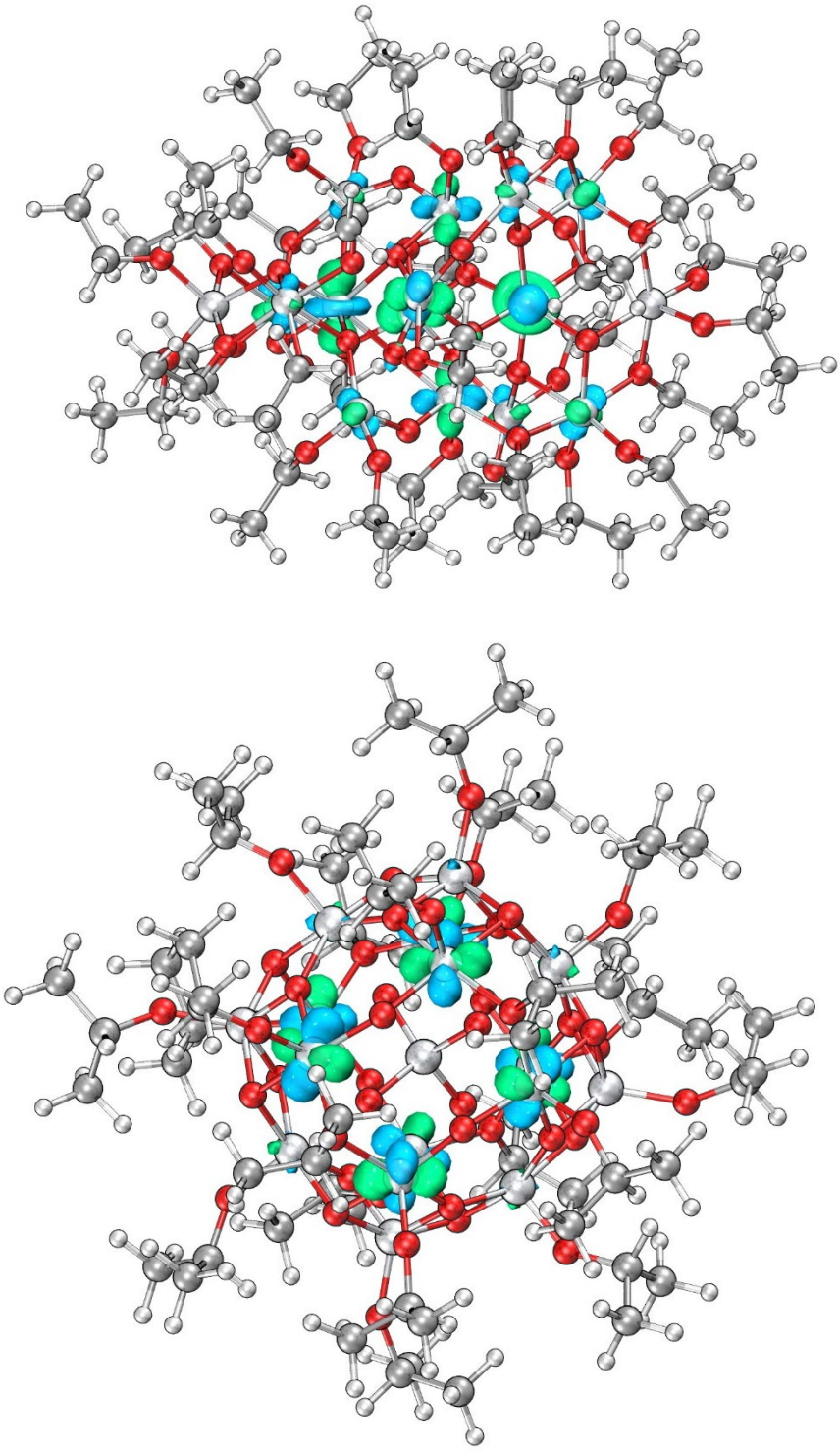

Figure S54. Calculated LUMO orbitals for **Ti_{16}** (top) and **Ti_{17}** (bottom)

Supporting note 1. Reported energy gaps of larger Ti-oxo clusters

A band-gap of 3.6 eV (linear extrapolation from DRS) is reported for the large cluster $[Ti_{42}O_{60}H_6(O^iPr)_{42}(OH)_{12})]$, which has a diameter of 1.5 nm, however, this structure adopts a fullerene-like empty cage, therefore, the cluster could be considered to be akin to a 1-D sheet.[20] The enormous carboxylate-supported cluster $Ti_{52}(\mu\text{-}OH)_2(\mu\text{-}O)_{14}(\mu_3\text{-}O)_{50}(\mu_4\text{-}O)_8(O_2CCH_2CH_3)_{34}(O^iPr)_{28}$, has a worm like structure that is 4 nm long but less than 1 nm across, this has a reported energy gap of 3.7 eV (by DRS), and may be considered a 1-D nanomaterial, with spatial confinement in two dimensions.[21, 22]

Supporting note 2. HOMO pinning experiments by use of phenoxide ligands.

Inspired by the work of Imai et al., who used a dopant phenoxide ligand to 'pin' the HOMO (or valence band) of quantum confined WO_3 systems,[23] we explored the absorption spectra of Ti complexes with phenoxide ligands. The 'pinned' HOMO level is intended to provide a consistent baseline against which all the LUMO (conduction band) energies can be compared across a series of systems. Equation 1 can be used to estimate the conduction band energy (LUMO), where E_{CB} is the conduction band energy, $E_{HOMO(phenol)}$ is the HOMO position of phenol (previously determined at 1.73 V vs NHE)[23] and E_{CT} is the energy of the charge transfer transition of an electron from the phenol HOMO to the LUMO (determined through the electronic absorption spectrum).

Equation 1 $\quad E_{CB} = E_{HOMO(phenol)} - E_{CT}$

To determine the appropriateness of this technique for small Ti(-oxo)-alkoxide systems, DFT calculations compared the HOMO and LUMO energies of monomeric $[Ti(O^iPr)_4]$ and $[Ti(O^iPr)_{4-x}(OPh)_x]$ (Fig. S55). The result for a single OPh ligand $[Ti(O^iPr)_3(OPh)]$ indicates that introducing phenoxide significantly effects the HOMO (–0.8 eV), which becomes ligand (π) based, but also stabilises the LUMO position (+0.3 eV) by mixing of the ligand π* with the Ti 3d orbitals, similarly to the influence of other dye ligands.[24] Therefore, caution is required when comparing the LUMO position of phenoxide substituted to phenoxide free clusters, and an estimate of ~0.3 eV stabilisation via π* mixing is used below. On increasing OPh content the HOMO remains similar but becomes slightly stabilised due to the electron withdrawing effect of phenoxide (versus isopropoxide), the LUMO is stabilised at a greater rate, indicating some enhanced mixing of ligand (π*) and 3d orbitals.

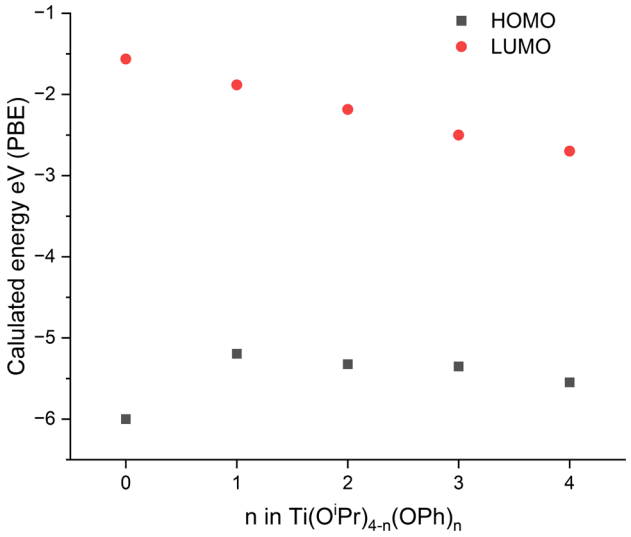

Figure S55. Calculated frontier orbital energies of $[Ti(O^iPr)_{4-n}(OPh)_n]$, indicating changes to both HOMO and LUMO upon the introduction of phenoxide ligands.

Alcohol exchange reactions can replace an alkoxide group with a phenoxide, a process driven by the enhanced acidity of phenol versus aliphatic alcohols. A study by Sanchez et al. demonstrates selective phenoxide exchange reactions with **Ti_{16}**.[25] Heating **Ti_{16}** with different ratios of phenol gave species with 4-16 of the 32 ethoxide ligands replaced with phenoxide. Samples with approximate formulas of $[Ti_{16}O_{16}(OEt)_{16}(OPh)_{16}]$ (**Ti_{16}^{OPh16}**), and $[Ti_{16}O_{16}(OEt)_{28}(OPh)_4]$ (**Ti_{16}^{OPh4}**) were prepared:

The synthesis of **Ti_{16}^{OPh16}** was adapted from a literature procedure.[25] **Ti_{16}** (200 mg, 0.08 mmol) was dissolved in 10 mL of dry toluene under a nitrogen atmosphere. Phenol (0.45 g, 4.9 mmol) was added, to give an orange solution, and the reaction stirred at 50 °C for 3 days. The solvent was removed under vacuum and the resulting solids washed with ~5 mL of dry acetonitrile to give an orange/yellow powder (isolated yield = 50 mg, 19% yield). **Ti_{16}^{OPh4}** was prepared using the same procedure but with 30 mg (0.32 mmol) of phenol (isolated yield of orange powder = 40 mg, 19%).

Ti_{16}^{OPh16} elemental analysis (predicted): C, 46.31 (47.56); H 4.89 (4.99)

Ti_{16}^{OPh4} elemental analysis (predicted): C, 36.02 (36.18); H 4.95 (6.07)

Both products showed a wide variety of ^{1}H NMR signals in the expected OEt and OPh regions, indicating a mixture of species and isomers. Integration of the ^{1}H NMR spectra suggests a OEt:OPh ratio of 1:1 and ~5:1 respectively. DOSY NMR spectroscopy revealed similar hydrodynamic diameters for **Ti_{16}** and **Ti_{16}^{OPh16}** (**Ti_{16}**, 1.7 nm (as expected from X-ray structure); **Ti_{16}^{OPh16}**, ~1.6 nm), consistent with the original report which suggests that ligand exchange results in retention of the core $Ti_{16}O_{16}$ structure.

The high concentration UV/vis spectrum of **Ti_{16}^{OPh16}** and **Ti_{16}^{OPh4}** collected with a consistent concentration of OPh ligands ([Ti] = 8.75 and 35 mM respectively) appear identical (Fig. S56a), both significantly red-shifted (indirect onset 2.38 ±0.05 eV) compared to **Ti_{16}**, indicating that the (phenoxide π to Ti 3d) LMCT absorption is consistent regardless of the number of phenoxide ligands attached to **Ti_{16}**. The low concentration spectra (Fig S56b) reveal the core oxygen to metal charge transfer has the same absorption onsets across the Ti_{16} species.

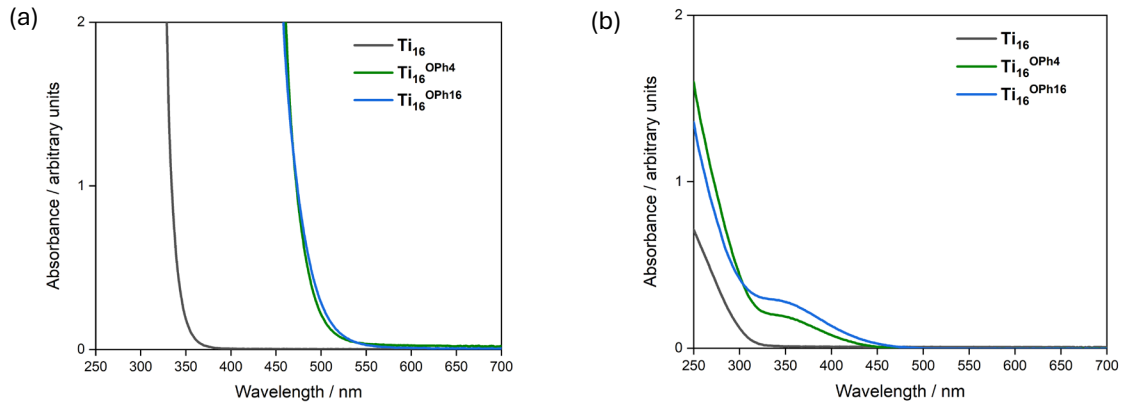

Figure S56. Solution UV/vis absorption spectra of phenoxide coordinated Ti_{16} complexes compared to **Ti_{16}**, a) **Ti_{16}** and **Ti_{16}^{OPh4}** [Ti] = 35 mM; **Ti_{16}^{OPh16}** [Ti] = 8.75 mM; b) all, [Ti] = ~0.11 mM

Assuming a HOMO position of ~1.73 eV vs NHE for **$Ti_{16}^{OPh16/4}$** the LUMO is then estimated at ~–0.65 eV vs NHE. Factoring in a ~0.3 eV LUMO stabilisation in the phenoxide compounds relative to **Ti_{16}**, the LUMO energy for **Ti_{16}** is therefore approximately ~–0.95 eV vs NHE (Fig S57). This result, whilst based on assumptions, is in good agreement with the estimation using electrochemical methods (-1.0 eV vs NHE, once converted from vs Fc/Fc+)

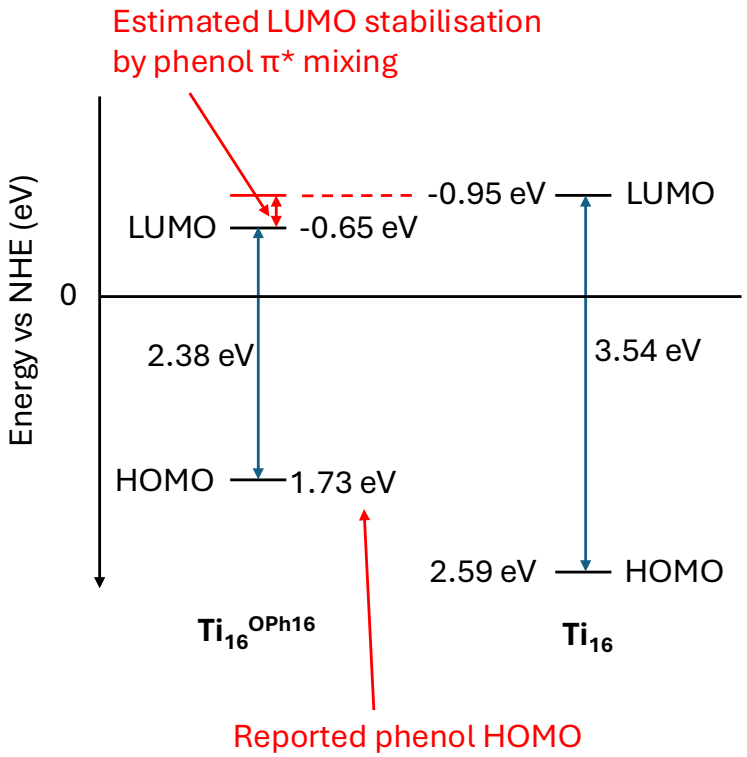

Figure S57. Diagram to show the predicted frontier energy levels of **Ti_{16}^{OPh16}** and **Ti_{16}** following assumptions made in phenol pinning experiments.

References

1. Krämer, T.; Tuna, F.; Pike, S. D., Photo-redox reactivity of titanium-oxo clusters: mechanistic insight into a two-electron intramolecular process, and structural characterisation of mixed-valent Ti(iii)/Ti(iv) products. *Chem. Sci.* **2019,** *10* (28), 6886-6898.
2. Stinghen, D.; Atzori, M.; Fernandes, C. M.; Ribeiro, R. R.; de Sá, E. L.; Back, D. F.; Giese, S. O. K.; Hughes, D. L.; Nunes, G. G.; Morra, E.; Chiesa, M.; Sessoli, R.; Soares, J. F., A Rare Example of Four-Coordinate Nonoxido Vanadium(IV) Alkoxide in the Solid State: Structure, Spectroscopy, and Magnetization Dynamics. *Inorg. Chem.* **2018,** *57* (18), 11393-11403.
3. Day, V. W.; Eberspacher, T. A.; Chen, Y.; Hao, J.; Klemperer, W. G., Low-nuclearity titanium oxoalkoxides: the trititanates [Ti3O](OPri)10 and [Ti3O](OPri)9(OMe). *Inorg. Chim. Acta* **1995,** *229* (1), 391-405.
4. Eslava, S.; Goodwill, B. P. R.; McPartlin, M.; Wright, D. S., Extending the Family of Titanium Heterometallic–oxo–alkoxy Cages. *Inorg. Chem.* **2011,** *50* (12), 5655-5662.
5. Day, V. W.; Eberspacher, T. A.; Klemperer, W. G.; Park, C. W., Dodecatitanates: a new family of stable polyoxotitanates. *J. Am. Chem. Soc.* **1993,** *115* (18), 8469-8470.
6. Schmid, R.; Mosset, A.; Galy, J., New compounds in the chemistry of Group 4 transition-metal alkoxides. Part 4. Synthesis and molecular structures of two polymorphs of [Ti16O16(OEt)32] and refinement of the structure of [Ti7O4(OEt)20]. *J. Chem. Soc., Dalton Trans.* **1991,** (8), 1999-2005.
7. Steunou, N.; Kickelbick, G.; Boubekeur, K.; Sanchez, C., A new polyoxo-alkoxo titanium cluster of the Keggin family: synthesis and characterization by X-ray diffraction and NMR spectroscopy. *J. Chem. Soc., Dalton Trans.* **1999,** (21), 3653-3655.
8. Campana, C. F.; Chen, Y.; Day, V. W.; Klemperer, W. G.; Sparks, R. A., Polyoxotitanates join the Keggin family: synthesis, structure and reactivity of [Ti18O28H][OBut]17. *J. Chem. Soc., Dalton Trans.* **1996,** (5), 691-702.
9. Day, V. W.; Eberspacher, T. A.; Klemperer, W. G.; Park, C. W.; Rosenberg, F. S., Solution structure elucidation of early transition metal polyoxoalkoxides using oxygen-17 NMR spectroscopy. *J. Am. Chem. Soc.* **1991,** *113* (21), 8190-8192.
10. Steunou, N.; Ribot, F.; Boubekeur, K.; Maquet, J.; Sanchez, C. m., Ketones as an oxolation source for the synthesis of titanium-oxo-organoclusters. *New J. Chem.* **1999,** *23* (11), 1079-1086.
11. Benedict, J. B.; Coppens, P., The Crystalline Nanocluster Phase as a Medium for Structural and Spectroscopic Studies of Light Absorption of Photosensitizer Dyes on Semiconductor Surfaces. *J. Am. Chem. Soc.* **2010,** *132* (9), 2938-2944.
12. Brown, S. E.; Mantaloufa, I.; Andrews, R. T.; Barnes, T. J.; Lees, M. R.; De Proft, F.; Cunha, A. V.; Pike, S. D., Photoactivation of titanium-oxo cluster [Ti6O6(OR)6(O2CtBu)6]: mechanism, photoactivated structures, and onward reactivity with O2 to a peroxide complex. *Chem. Sci.* **2023,** *14*, 675-683.
13. Brown, S. E.; Warren, M. R.; Kubicki, D. J.; Fitzpatrick, A.; Pike, S. D., Photoinitiated Single-Crystal to Single-Crystal Redox Transformations of Titanium-Oxo Clusters. *J. Am. Chem. Soc.* **2024,** *146* (25), 17325-17333.
14. Makuła, P.; Pacia, M.; Macyk, W., How To Correctly Determine the Band Gap Energy of Modified Semiconductor Photocatalysts Based on UV–Vis Spectra. *J. Phys. Chem. Lett.* **2018,** *9* (23), 6814-6817.
15. Macpherson, J. V., A practical guide to using boron doped diamond in electrochemical research. *Phys. Chem. Chem. Phys.* **2015,** *17* (5), 2935-2949.
16. Bradley, D. C.; Holloway, C. E., Nuclear magnetic resonance and cryoscopic studies on some alkoxides of titanium, zirconium, and hafnium. *J. Chem. Soc. A.* **1968,** (0), 1316-1319.
17. Babonneau, F.; Doeuff, S.; Leaustic, A.; Sanchez, C.; Cartier, C.; Verdaguer, M., XANES and EXAFS study of titanium alkoxides. *Inorg. Chem.* **1988,** *27* (18), 3166-3172.

18. Boyle, T. J.; Alam, T. M.; Mechenbier, E. R.; Scott, B. L.; Ziller, J. W., Titanium(IV) Neopentoxides. X-ray Structures of Ti3(μ3-O)(μ3-Cl)(μ-OCH2CMe3)3(OCH2CMe3)6 and [Ti(μ-OCH2CMe3)(OCH2CMe3)3]2. *Inorg. Chem.* **1997,** *36* (15), 3293-3300.
19. Satoh, N.; Nakashima, T.; Kamikura, K.; Yamamoto, K., Quantum size effect in TiO2 nanoparticles prepared by finely controlled metal assembly on dendrimer templates. *Nat. Nanotechnol.* **2008,** *3*, 106.
20. Gao, M.-Y.; Wang, F.; Gu, Z.-G.; Zhang, D.-X.; Zhang, L.; Zhang, J., Fullerene-like Polyoxotitanium Cage with High Solution Stability. *J. Am. Chem. Soc.* **2016,** *138* (8), 2556-2559.
21. Fang, W.-H.; Zhang, L.; Zhang, J., A 3.6 nm Ti52–Oxo Nanocluster with Precise Atomic Structure. *J. Am. Chem. Soc.* **2016,** *138* (24), 7480-7483.
22. Peng, H.; Li, J., Quantum Confinement and Electronic Properties of Rutile TiO2 Nanowires. *J. Phys. Chem. C* **2008,** *112* (51), 20241-20245.
23. Suzuki, T.; Watanabe, H.; Oaki, Y.; Imai, H., Tuning of photocatalytic reduction by conduction band engineering of semiconductor quantum dots with experimental evaluation of the band edge potential. *Chem. Commun.* **2016,** *52* (36), 6185-6188.
24. Sokolow, J. D.; Trzop, E.; Chen, Y.; Tang, J.; Allen, L. J.; Crabtree, R. H.; Benedict, J. B.; Coppens, P., Binding Modes of Carboxylate- and Acetylacetonate-Linked Chromophores to Homodisperse Polyoxotitanate Nanoclusters. *J. Am. Chem. Soc.* **2012,** *134* (28), 11695-11700.
25. Fornasieri, G.; Rozes, L.; Le Calvé, S.; Alonso, B.; Massiot, D.; Rager, M. N.; Evain, M.; Boubekeur, K.; Sanchez, C., Reactivity of Titanium Oxo Ethoxo Cluster [Ti16O16(OEt)32]. Versatile Precursor of Nanobuilding Block-Based Hybrid Materials. *J. Am. Chem. Soc.* **2005,** *127* (13), 4869-4878.